J. Fluid Mech. (1987), *vol.* 175, *pp.* 363–394
Printed in Great Britain

On rotating disk flow

By JOHN F. BRADY† AND LOUIS DURLOFSKY
Department of Chemical Engineering, Massachusetts Institute of Technology, Cambridge, MA 02139, USA

(Received 7 July 1986)

The relationship of the axisymmetric flow between large but finite coaxial rotating disks to the von Kármán similarity solution is studied. By means of a combined asymptotic–numerical analysis, the flow between finite disks of arbitrarily large aspect ratio, where the aspect ratio is defined as the ratio of the disk radii to the gap width separating the disks, is examined for two different end conditions: a 'closed' end (shrouded disks) and an 'open' end (unshrouded or free disks). Complete velocity and pressure fields in the flow domain between the finite rotating disks, subject to both end conditions, are determined for Reynolds number (based on gap width) up to 500 and disk rotation ratios between 0 and -1. It is shown that the finite-disk and similarity solutions generally coincide over increasingly smaller portions of the flow domain with increasing Reynolds number for both end conditions. In some parameter ranges, the finite-disk solution may not be of similarity form even near the axis of rotation. It is also seen that the type of end condition may determine which of the multiple similarity solutions the finite-disk flow resembles, and that temporally unstable similarity solutions may qualitatively describe steady finite-disk flows over a portion of the flow domain. The asymptotic–numerical method employed has potential application to related rotating-disk problems as well as to a broad class of problems involving flow in regions of large aspect ratio.

1. Introduction

Flows driven by rotating disks have constituted a major field of study in fluid mechanics for the better part of this century. These flows have technical applications in many areas, such as rotating machinery, lubrication, viscometry, computer storage devices and crystal growth processes. They are of special theoretical interest, however, because they represent one of the few examples for which there is an exact solution to the Navier–Stokes equations.

This was first recognized by von Kármán (1921) who considered the problem of a disk of infinite extent rotating in an unbounded, quiescent fluid. By assuming a self-similar, axisymmetric velocity profile, he was able to reduce the full equations of motion to a pair of nonlinear ordinary differential equations. Cochran (1934) obtained the first accurate numerical solution to von Kármán's equations; his well-known solution shows the action of the disk as a centrifugal fan, throwing fluid out radially and drawing it in axially. Bödewadt (1940) extended von Kármán's analysis to treat the problem of flow above a stationary disk with the outer flow in solid-body rotation. Batchelor (1951) generalized the analyses of von Kármán and Bödewadt to include one- and two-parameter families of solutions having a mathe-

† Present address: Department of Chemical Engineering, California Institute of Technology, Pasadena, CA 91125, USA.

matical structure very similar to that of von Kármán's. The one-parameter family corresponds to the flow above a single infinite disk rotating at angular velocity Ω_0 with the fluid at infinity in solid-body rotation of angular velocity Ω_1. The ratio of these angular velocities, $s = \Omega_1/\Omega_0$, is the single parameter. The two-parameter family of solutions describes the flow between two infinite, coaxial rotating disks; in addition to the ratio of the angular velocities of the disks s an additional parameter, the Reynolds number, $Re = \Omega_0 H^2/\nu$ based on the gap width between the disks H, appears.

Batchelor did not attempt to solve the similarity equations he derived but rather discussed qualitatively their expected features. For the flow between two infinite disks, he argued that, at high Reynolds number for $s \geqslant 0$, the fluid between the disks would rotate with a constant angular velocity and that boundary layers would form at both disks. Stewartson (1953) obtained solutions to the similarity equations for flow between two rotating disks as a power series in the Reynolds number. Based on the trends observed as the Reynolds number was increased, he concluded that, for one disk rotating and the other stationary ($s = 0$), a boundary layer would form only at the rotating disk and the core would not rotate. The limiting solution, therefore, would be the von Kármán free-disk solution. Stewartson also predicted that the fluid in the core would not rotate when the disks rotate in the opposite sense.

Following the papers of Batchelor and Stewartson and continuing through to the present, there has been a large body of published literature concerning the flow between rotating disks. It is not our intent here to review this; we shall only briefly discuss a few of the papers that are most applicable to our study. A more extensive discussion can be found in Durlofsky (1986). Some of the earlier work (pre-1968) is discussed by Greenspan (1980); more recent analytical and numerical work is reviewed by Parter (1982). The recent review of Zandbergen & Dijkstra (1987) provides an extensive survey of theoretical and numerical papers concerning rotating-disk flows.

Early numerical solutions by Lance & Rogers (1962) and Pearson (1965) seemed to indicate that the Batchelor form was the proper limiting solution for the flow between a rotating disk and a stationary disk. This question was clarified, however, when Mellor, Chapple & Stokes (1968) demonstrated that both the Batchelor and Stewartson solutions, as well as many others, exist at high Reynolds number for $s = 0$. The Batchelor solution evolves from the zero-Reynolds-number solution; the Stewartson solution does not appear until $Re \approx 217$.

Since the work of Mellor *et al.*, many investigators, most notably Nguyen, Ribault & Florent (1975), Roberts & Shipman (1976), Holodniok, Kubicek & Hlavacek (1977, 1981) and Szeto (1978), have studied von Kármán's similarity equations for flow between infinite rotating disks and have shown their structure to be extremely complex. Szeto reported the most extensive calculations on the similarity equations describing flow between two infinite coaxial rotating disks, spanning s from -1 to $+1$ and Re from 0 to 1000. Several interesting features of the solution structure became apparent. Specifically, Szeto demonstrated the existence of a uniform region of uniqueness: for $Re < 55$ and all values of s the solution is unique; for $Re > 55$ the solution is non-unique for all s. He also showed that, for any value of s, a single continuous solution extending from zero to infinity in Re exists. Due to limit points in s, however, none of these continuous solution branches exists for all s; i.e. no continous sheet of solutions spanning all Re and all s exists.

Szeto found as many as 19 solutions to the similarity equations in some parameter ranges, many of which correspond to rather unusual (perhaps aphysical) velocity

profiles. Despite this myriad of solutions and critical points, only one bifurcation was observed: for exact counter-rotation ($s = -1$) at $Re = 119.8$, symmetric, two-cell solutions bifurcate supercritically to asymmetric, two-cell solutions. Szeto also analysed the temporal stability of many of the solution branches; among his findings are that the $s = 0$ Batchelor solution is stable, the $s = 0$ Stewartson solution is unstable, and the symmetric solution at $s = -1$ loses stability to the bifurcating, asymmetric solutions at $Re = 119.8$.

The solution multiplicity of the rotating-disk similarity equations, as well as the aphysical velocity fields that many of the solution branches display, call into question the ability of the similarity solution to describe the real flow it is intended to represent – the flow between finite rotating disks. It is not apparent from the similarity analysis which, if any, of the similarity solutions in a given parameter range might describe such a flow.

The purpose of this work is to investigate the validity of the similarity solution in describing the flow between two finite rotating disks. Toward this end, we use a combined asymptotic–numerical analysis that allows us to examine the flow between finite disks of arbitrarily large aspect ratio. The aspect ratio is defined as the ratio of the disk radii L to the gap width separating them H. The results of this analysis, considered in the light of the temporal stability of the similarity solution, enable us to elucidate the relationship between the similarity solution and the real flow it is intended to represent.

The similarity analysis applies to disks that are infinite in extent and therefore no 'end condition' can be imposed. For the proper analysis of flow between disks of finite extent, however, an end condition is required. Indeed, it is the end that distinguishes between finite and infinite disks. As we shall show in §2, by means of an asymptotic analysis we can analyse the effects of the end in a general way for arbitrarily large aspect ratios. Upon appropriately non-dimensionalizing the equations of motion and taking the limit as the aspect ratio becomes large, it will be seen that the aspect ratio drops out of all equations and boundary conditions. Thus, through this approach we avoid the problem of considering any specific aspect ratio and can then determine which, if any, of the similarity solutions gives a valid description of the flow between rotating disks of finite extent and over what portion of the flow domain this agreement exists. Let us define precisely what we mean by the similarity solution giving a 'valid' description of the flow between finite rotating disks. For the similarity solution to be considered valid at a given radial position, it must quantitatively agree with the finite-disk solution at *all* axial locations corresponding to this radial position.

In this study, two types of end conditions are considered: a 'closed' end, which corresponds to disks enclosed by a cylinder (shrouded disks), and an 'open' end, which corresponds to the disks surrounded by an unbounded fluid (unshrouded or free disks). Our approach is analogous to those of Brady & Acrivos (1982) and Brady (1984) in their studies of the flow in a long but finite channel or tube whose surface either moves with a velocity linear in the streamwise coordinate or is uniformly porous.

In the past, many studies (e.g. Pao 1970, 1972; Lugt & Haussling, 1973; Adams & Szeri 1982; Szeri *et al.* 1983*a*,*b*; Dijkstra & van Heijst 1983; Harriott & Brown 1984) have addressed the general problem of axisymmetric flow between finite rotating disks enclosed by a cylinder but, with the exception of that of Dijkstra & van Heijst, none has considered both large aspect ratios ($L/H > \sim 10$), where the similarity solution might be expected to be applicable, and high Reynolds number ($Re \gtrsim 200$), probably because the numerical resolution of the flow near the outer edge

poses a difficult numerical problem under these conditions. The work of Harriott & Brown, where the flow in a differentially rotated, non-deformable cylindrical drop with aspect ratio ranging from less than one to three is considered, is significant in that solution multiplicity is observed. In the case of exact counter-rotation ($s = -1$), for example, Harriott & Brown observed both symmetric and asymmetric solutions connected by a supercritical bifurcation.

To recover the similarity solution over any part of the flow domain, it is apparent that the end must be further removed, i.e. a larger aspect ratio is required. Dijkstra & van Heijst (1983) performed extensive numerical calculations at an aspect ratio of 14 for Reynolds number up to 1000. Because the numerical resolution of the details of the flow near the outer edge for such a large aspect ratio posed a difficult numerical problem, Dijkstra & van Heijst were forced to skew their finite-difference mesh toward the disk edge for their numerical scheme to work well. As a result, their mesh was extremely sparse near the axis of rotation, making comparison with a similarity solution difficult. They considered $s = 0$ and several values of negative s; in some cases agreement with the similarity solution was established. The objective of the work of Dijkstra & van Heijst was apparently not to make a systematic, quantitative comparison between their results and the similarity solution. Even with better mesh resolution near the axis of rotation, an approach such as theirs might still not strictly determine the validity of the similarity solutions. Though considerably larger than one, an aspect ratio of 14 used by Dijkstra & van Heijst is not necessarily large enough. If, in some parameter ranges, their results differ from the similarity solution over the entire flow domain, the question of whether a larger aspect ratio might reconcile this difference arises, and this uncertainty may persist for all finite aspect ratios. Our approach avoids this problem in that we consider the flow between rotating disks of arbitrarily large, but finite, aspect ratio. This point will become clear in the asymptotic analysis in §2.

Many experimental studies of the flow between rotating disks have been performed. We shall comment only on the results that are applicable to our study. Experiments on the flow between a rotating and a stationary disk ($s = 0$) were conducted by Schultz-Grunow (1935), Stewartson (1953), Picha & Eckert (1958), Mellor *et al.* (1968), Bien & Penner (1970), Szeri *et al.* (1983*b*) and Dijkstra & van Heijst (1983). From these studies, it is apparent that, at high Reynolds number, the disk housing (shrouded or unshrouded disks) fundamentally affects the flow field over the entire domain. If the disks are unshrouded, experiments indicate that, at high Reynolds number, the fluid core displays no observable angular motion and little radial motion. If the disks are shrouded, however, there is a definite angular motion in the core as well as a radial motion.

Picha & Eckert and Dijkstra & van Heijst conducted experiments with both disks rotating. At an aspect ratio of nine, for both shrouded and unshrouded disks at high Re, Picha & Eckert observed no rotation in the fluid core when the disks were counter-rotated. Dijkstra & van Heijst performed extensive experiments with shrouded disks at an aspect ratio of 14. They varied Re from 50 to 1000 and s from 0 to -0.825. Their high-Re results at $s = -0.6$ and $s = -0.45$ show no angular velocity in the core; at $s = -0.15$, however, they did observe a definite core angular velocity. Dijkstra & van Heijst were also able to locate the stagnation point, where the dividing streamline meets the slower moving disk, for $s < 0$ as a function of Reynolds number over a large range of s and Re.

In §2 we formulate the equations and boundary conditions for the similarity solution and the asymptotic–numerical analysis for flow between large but finite

disks. From the asymptotic analysis, it is clear that the disks, though finite, can be arbitrarily large because, once small terms in the equations of motion are neglected, the disk radii do not appear in the equations of motion, the boundary conditions or the Reynolds number. Because our asymptotic analysis avoids the need to resolve the details of the flow field near the outer edge, our numerical routine is fast and accurate and the entire flow domain is well resolved. The asymptotic–numerical method can potentially be applied to many related rotating-disk problems, as well as to other large-aspect-ratio problems where the effect of an end or a turning region needs to be accounted for in a general way but the details of the flow in this region are not essential or desired.

Although our analysis is valid for $-1 \leqslant s < 1$, we shall present results, in §3, only for $-1 \leqslant s \leqslant 0$. For all values of s considered, the effect of the end on the flow between finite rotating disks is seen to increase with increasing Reynolds number; i.e. the flow deviates from similarity form over a greater portion of the flow domain as Re is increased. This is in itself a significant result. One might expect that given a finite-disk arrangement, the effect of the end (in a dimensionless sense) could be reduced and eventually confined to a region in the immediate vicinity of the end by either getting larger disks or reducing the spacing between them. Our asymptotic analysis and numerical results show, however, that for arbitrarily large disks the effect of the end is not, in general, confined to a region near the end.

For exact counter-rotation, $s = -1$, the symmetric, Stewartson similarity solution is seen to give a valid description of the finite-disk flow over some portion of the domain for $Re \leqslant 500$ (the largest Re considered) for the open-end flows and for $Re \leqslant 350$ for the closed-end flows. This similarity solutions is, however, temporally unstable for $Re > 119.8$, so we have the rather surprising result that the flow between finite rotating disks can be described by an unstable similarity solution. This apparent discrepancy is resolved by considering the temporal stability of the similarity solution, which indicates that only disturbances that are asymmetric about the midline between the disks will excite the unstable mode. The introduction of such disturbances to the $s = -1$ flows results in a change in the flow structure which invalidates the similarity solution as a local description of the flow near the axis of rotation.

For the case of one disk rotating and the other stationary, $s = 0$, the end condition is seen to determine which similarity solution the flow resembles at high Re. Though strict quantitative agreement with the similarity solution at high Re is not achieved in either case, the closed-end flows resemble the Batchelor solution while the open-end flows resemble the Stewartson solution. For $Re \leqslant 80$, both the open- and closed-end flows agree with the Batchelor solution near the axis of rotation. As the Reynolds number is increased, the open end-flows tend away from the Batchelor solution and toward the Stewartson solution, while the closed-end flows continue to resemble the Batchelor solution up to $Re = 1000$, the largest Re considered.

Next we consider strong counter-rotation, $s = -0.8$. These results qualitatively resemble the $s = -1$ results, though several new features appear. For $Re < 120$ both the open- and closed-end flows are described by the similarity solution near the axis of rotation. For $Re > 120$, the closed-end flows do not agree with any similarity solution anywhere in the flow domain. The open-end flows for $Re \geqslant 200$ are, however, described by two different similarity solutions in two different regions of the flow domain.

Finally, we compare some of our numerical work with experimental data from the literature. The good agreement obtained indicates that our analysis, though strictly

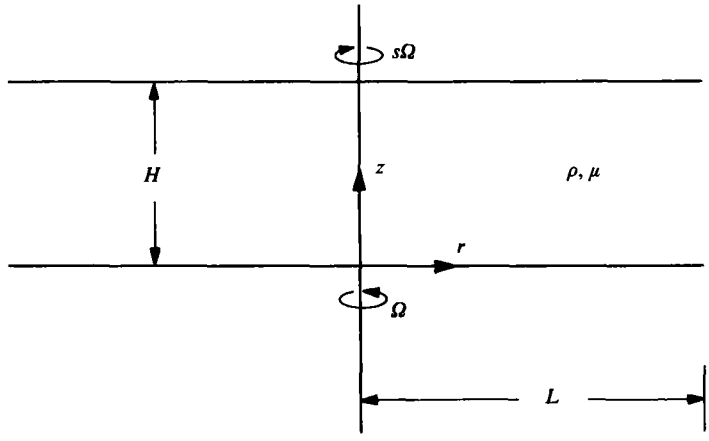

FIGURE 1. Schematic diagram for the flow between two coaxial rotating disks. For the similarity solution, $L/H \to \infty$.

valid only for very large aspect ratios, accurately describes realizable flows at more moderate aspect ratios, even near the outer edge. In addition, our numerical results are consistently in agreement with qualitative experimental observations, and explain observed differences in the flow structure as the ratio of angular velocities s is varied.

2. Problem formulation

2.1. *Similarity solution*

As shown in figure 1 we denote the spacing between the disks by H, the angular velocity of the bottom disk by Ω, the angular velocity of the top disk by $s\Omega$, the fluid viscosity by μ and its density by ρ. For disks of infinite radius ($L/H \to \infty$), the Navier–Stokes equations admit an exact solution of the similarity form

$$u = -\tfrac{1}{2}rf'(z), \quad v = rg(z), \quad w = f(z), \tag{1a,b,c}$$

$$p = p_0(z) + \tfrac{1}{4}(\beta/Re)\, r^2, \tag{1d}$$

where u, v and w are the radial, azimuthal and axial components of the velocity field, β is a constant and $Re = \rho\Omega H^2/\mu$ is the Reynolds number. The similarity functions f and g satisfy the ordinary differential equations

$$f''' + \beta = Re\,[-\tfrac{1}{2}(f')^2 + ff'' + 2g^2], \tag{2a}$$

$$g'' = Re\,[fg' - gf'], \tag{2b}$$

subject to no-slip boundary conditions at both disks

$$f(0) = f'(0) = 0, \quad g(0) = 1, \tag{3a}$$

$$f(1) = f'(1) = 0, \quad g(1) = s. \tag{3b}$$

The sixth boundary condition serves to determine the unknown pressure coefficient β. Szeto (1978) showed that only $|s| \leqslant 1$ and $Re \geqslant 0$ need be considered; taking $|s| > 1$ simply corresponds to interchanging the disks and rescaling Re.

Many different numerical schemes have been used to solve the two-point boundary-

value problem posed by (2) and (3). We first differentiated (2*a*) with respect to z to eliminate β and then solved the resulting sixth-order system using the finite-element method with cubic Hermite basis functions and Newton iterations. An arc-length continuation procedure was used to trace solution branches around limit points.

2.2. *Flow between rotating disks of finite extent: asymptotic analysis*

We now consider the problem for the flow between rotating disks of large but finite radii L with $L/H \gg 1$. The natural scalings are: $r \sim O(L)$; $z \sim O(H)$; u and $v \sim O(\Omega L)$; w, from continuity, $\sim O(\Omega H)$ and p, scaled with the inertial terms, $\sim O(\rho\Omega^2 L^2)$. For axisymmetric flow, in the limit of large aspect ratio, $L/H \gg 1$, the dimensionless equations of motion and continuity become

$$u\frac{\partial u}{\partial r}-\frac{v^2}{r}+w\frac{\partial u}{\partial z}+\frac{\partial p}{\partial r}=\frac{1}{Re}\left\{\frac{\partial^2 u}{\partial z^2}+O\left[\left(\frac{H}{L}\right)^2\right]\right\}, \tag{4a}$$

$$u\frac{\partial v}{\partial r}+\frac{uv}{r}+w\frac{\partial v}{\partial z}=\frac{1}{Re}\left\{\frac{\partial^2 v}{\partial z^2}+O\left[\left(\frac{H}{L}\right)^2\right]\right\}, \tag{4b}$$

$$\frac{\partial p}{\partial z}=O\left[\frac{1}{Re}\left(\frac{H}{L}\right)^2,\left(\frac{H}{L}\right)^2\right], \tag{4c}$$

$$\frac{1}{r}\frac{\partial}{\partial r}ru+\frac{\partial w}{\partial z}=0, \tag{4d}$$

where Re is again $\rho\Omega H^2/\mu$. The boundary conditions in z are as before (cf. (3))

$$u(r,0)=w(r,0)=0, \quad v(r,0)=r, \tag{5a}$$

$$u(r,1)=w(r,1)=0, \quad v(r,1)=rs. \tag{5b}$$

The boundary conditions in r remain to be specified.

Equation (4) is similar to the equations derived by Brady & Acrivos (1982) for flow in a finite channel or tube with an accelerating surface velocity and in Brady (1984) for the flow in a finite channel or tube with a porous wall. For these types of problems, the governing equations are seen to be similar to the boundary-layer equations, except that the transverse (in this case axial) coordinate is $O(1)$ and the Reynolds number appears as a parameter. Furthermore, the large lengthscale L does not appear in the equations (once terms of $O[(H/L)^2]$ have been neglected), in the Reynolds number, in the boundary condition in z or, as we shall see, in the boundary conditions in r. Therefore, as long as $L/H \gg 1$, the absolute scale of L is immaterial; the analysis is valid for disks of arbitrarily large radii. Note that (4) and (5) admit a solution of the similarity form (1).

To complete the specification of the problem, we need to formulate conditions at the ends of the disks ($r = 1$ in dimensionless variables) and, as we shall see, possibly near the axis of rotation ($r = 0$). We could simply specify an arbitrary, mass-conserving velocity field at $r = 1$ but this would not, in general, correspond to a physically realistic end condition. The end conditions we wish to consider are those of a closed end, where the disks are enclosed by a cylinder, and an open end, where the disks are surrounded by an infinite, unbounded fluid.

2.2.1. *Closed end*

To formulate a condition for the closed end, we follow the approach of Brady (1984) and Brady & Acrivos (1982). As discussed in these papers, (4) (or its analogue)

is not necessarily valid within an $O(H/L)$ region near $r = 1$ because, near the end, the r-variation in the flow occurs on the scale of H rather than L. Equation (4), therefore, should be viewed as applying to the flow in the $O(1)$ 'outer' region whose solution must match with the solution to an equation valid in the $O(H/L)$ 'inner' region, near the ends of the disks. The determination of the complete flow field in this inner region would pose a difficult numerical problem but, as we shall show, this is not necessary because it serves only to provide a boundary condition for (4). Thus, the conditions at $r = 1$ that we shall impose on (4) are not true boundary conditions for the full equations of motion, but rather matching conditions between the inner and outer regions.

To analyse the region near the end $r = L$ (in dimensional variables), we define a new non-dimensional variable, $\sigma = (L-r)/H$, measuring the distance from the end on the scale of H. In order to match with the flow in the outer region ($r \sim O(L)$), the velocities u and v is this inner region remain $O(\Omega L)$, and, from continuity, w becomes large, $O(\Omega L)$ also. Thus, in this inner region, with $\sigma \sim O(1)$, the flow is inviscid, with an effective Reynolds number of $Re(L/H)$, and locally two-dimensional, i.e. curvature effects are negligible. Hence, apart from the angular swirling motion, we have a two-dimensional inviscid 'turning' region at $r = 1$, where the fluid thrown outward by the spinning disk(s) collides with the closed end, turns around and flows back towards $r = 0$. The only situation in which the flow in this $O(H/L)$ region would not be inviscid is if the disks were in near solid-body rotation ($s \approx 1$). Because we are interested only in $-1 \leqslant s \leqslant 0$, we shall not concern ourselves with this case. There are of course boundary layers adjacent to the disks and on the outer cylindrical wall in this inviscid turning region, but these will scale as $\{Re(L/H)\}^{-\frac{1}{2}}$ and therefore will not contribute to the matching condition with the outer region to leading order in $L/H \gg 1$.

In a two-dimensional inviscid flow, vorticity is conserved along streamlines, i.e.

$$\frac{\partial^2 \Psi}{\partial \sigma^2} + \frac{\partial^2 \Psi}{\partial z^2} = -\omega(\Psi), \tag{6}$$

where Ψ is the two-dimensional stream function ($u = \partial\Psi/\partial z$, $w = -\partial\Psi/\partial\sigma$) and the vorticity ω is a function of Ψ only. Because (6) only serves to provide a matching condition between the inviscid end region and the main flow governed by (4), we are only interested in its behaviour as the outer region is approached, i.e. as $\sigma \to \infty$. The mismatch in the axial velocity w between the two regions requires that it vanish as $\sigma \to \infty$. Thus, (6) becomes on matching

$$\frac{\partial^2 \Psi}{\partial z^2} = -\omega(\Psi), \tag{7}$$

which, if we consider a point z_0 at which $u = 0$, implies that $u(\sigma \to \infty, z)$ must be antisymmetric about z_0.

For the moment, let us assume that, near the disk edge, only the bottom disk throws fluid out in the positive radial direction. This will of course be the case when $s = 0$ and is also the case for slightly negative s at sufficiently low Reynolds number. Equation (7) implies that upon matching the radial velocity is antisymmetric about a point z_0, and, in order to conserve mass, we must additionally require that $z_0 \leqslant \frac{1}{2}$.

Because z_0 cannot be determined precisely at leading order, the matching condition between the inviscid region and the $O(1)$ region is not determined uniquely. Though any $z_0 \leqslant \frac{1}{2}$ is an acceptable choice, $z_0 = \frac{1}{2}$ seems to be the most reasonable. Choosing

$z_0 < \frac{1}{2}$ implies that the returning fluid will be displaced from the top disk and a region of stagnant fluid will exist near the top disk. Although seemingly aphysical, a flow of this nature is dynamically possible. In this regard, however, it should be noted that Dijkstra & van Heijst (1983), who fully resolve the $r = 1$ end region, in no cases report such behaviour. Thus, we choose $z_0 = \frac{1}{2}$, allowing the end condition for u to be simply stated as

$$u(z) = -u(1-z), \quad 0 \leqslant z \leqslant \tfrac{1}{2}, \quad \text{at } r = 1. \tag{8}$$

In an inviscid axisymmetric flow with swirl, the azimuthal velocity is given by (Batchelor 1967)

$$v = rC(\Psi), \tag{9}$$

which, at the disk end $r = 1$, reduced to $v = C(\Psi)$. This simply states that angular velocity is conserved along streamlines. Along with (7), this implies that $v(\sigma \to \infty, z)$ is symmetric about the point z_0. So, for $z_0 = \frac{1}{2}$, the end condition for v is

$$v(z) = v(1-z), \quad 0 \leqslant z \leqslant \tfrac{1}{2}, \quad \text{at } r = 1. \tag{10}$$

For the boundary-layer-like equations (4) no condition in r is needed for the axial velocity.

The end condition derived from the inviscid analysis is consistent with intuition. Physically, we expect the fluid thrown out by the bottom disk to traverse up the sidewall, while maintaining its angular velocity, and re-emerge at the top disk. This is precisely what the closed-end turning-region analysis specifies. Note that, because the flow near the enclosed end is inviscid, it make no difference, to a first approximation, whether the enclosure itself rotates or not. This result is in agreement with the experimental observations of Dijkstra & van Heijst (cf. §3.4).

When both disks throw fluid out in the positive radial direction near the disk end, as is the case for s near -1 or for slightly negative s at sufficiently high Reynolds number, the analysis is more involved. In this case, there are two z_0 values, one associated with the flow from the top disk and one with the flow from the bottom disk. Neither is determined uniquely from the inviscid analysis. Physically, the fluid thrown out by the bottom disk traverses up the sidewall and the fluid from the top disk traverses down. Both streams maintain their angular velocity. When these two streams collide, they turn and flow radially inward. The precise location of this collision point, which would determine both z_0 values, is uncertain. In the results we shall present, we have assumed that the location of this collision is determined by the ratio of the widths of the two colliding jets, which is roughly proportional to the ratio of the mass flow rates. This assumption allows us to determine the z_0 values and to apply boundary conditions at $r = 1$. The non-uniqueness of the colliding inviscid streams allows other possibilities. While other choices affect the flow locally near the edge – within two or three grid points – they do not influence the bulk of the flow in the $O(1)$ region between the disks. The most important elements in the end condition are conservation of vorticity and angular velocity along stream-lines. The details of how this is accomplished are relatively unimportant.

2.2.2. *Open end*

For an open end, the analysis at $r = 1$ is considerably different because the streamlines originate outside the disks. The fluid thrown outward past $r = 1$ by the spinning disk(s) must be replaced by the surrounding fluid in order to conserve mass. Thus, the surrounding fluid is simply drawn into the flow domain by a radial pressure gradient. Because $\partial p/\partial z = 0$ everywhere in the flow domain, the incoming fluid is of

uniform radial velocity and, because the surrounding fluid is quiescent, the angular velocity of the incoming fluid is zero. The case where the surrounding fluid rotates with a specified angular velocity can also be examined. Thus, for an open end the matching conditions for (4) are simply that fluid moving in the positive radial direction exits and a uniform, mass-conserving radial flow with zero angular velocity returns. Again, the precise details of how the fluid is returned are relatively unimportant.

As discussed by Brady (1984) and Brady & Acrivos (1982), an inviscid 'collision' region may arise at $r = 0$ at sufficiently large Reynolds number. Such an inviscid region occurs when the radial velocity of the returning fluid does not decay to zero rapidly enough as $r \to 0$. As was the case for the inviscid end region near $r = 1$, we are again not concerned with the details of the motion within this region but only with the matching condition it provides for the boundary-layer-like equations (4). This matching condition is derivable from an inviscid analysis much like that described for the closed-end condition. Though the two analyses are similar, the structure of the $r = 0$ collision region is more complex because the scaling for the velocities is not known *a priori* and because the effect of curvature cannot be neglected. However, the resulting matching condition, which supplies us with a 'consistency' condition (the flow in the $O(1)$ domain must be consistent with this analysis if a collision region forms), turns out to be of a form identical with the $r = 1$ closed-end matching condition. We use the word consistency for the condition at $r = 0$ because the boundary-layer-like equations (4), being parabolic in r, only require one boundary condition in r, the end condition at $r = 1$. However, to be consistent with the full, elliptic Navier–Stokes equations, the solution to (4) must also match with an appropriate solution as $r \to 0$.

The problem formulation is now complete. We have specified the governing equations (4), axial boundary conditions (5), radial boundary conditions at $r = 1$ for the two types of ends, and a consistency condition at $r = 0$. The numerical solution procedure is similar to that used by Brady (1984) and Brady & Acrivos (1982). The time-dependent terms are added to (4) and a finite-difference scheme, using space-centred differences in the axial direction and upwind differences in the radial direction, is used to solve the resulting transient problem. The integration in time is implicit in the axial direction but explicit in the radial direction. A uniformly spaced mesh of 51×51 is typically used, though little difference in the solution is observed with 26×26 or 101×101 meshes. The unknown pressure gradient is determined by imposing the constraint of no net radial flux. The equations are integrated in time until a steady solution is reached; at high Re this generally requires a dimensionless time of about 30 to 40, the time being made non-dimensional with Ω^{-1}.

The conditions at $r = 1$ and 0 evolve in time along with the rest of the solution. To determine the boundary conditions at $r = 1$, the radial and azimuthal velocities are linearly extrapolated from the last two grid points to $r = 1$. Regions where the extrapolated radial velocity is positive are left unchanged. Regions where the extrapolated radial velocity is negative represent the returning fluid and are adjusted according to the collision region analysis. For the open-end condition, the negative velocity is adjusted to be uniform subject to the constraint of conservation of mass. The angular velocity of the incoming fluid is set to zero. For the closed-end condition, the returning flow is adjusted such that the radial velocity profile is antisymmetric about the point (or points) z_0 and the azimuthal velocity symmetric. Under some conditions, the extrapolated radial velocity is positive in only a small region near the bottom disk (say from $z = 0$ to a, $a < \frac{1}{2}$). Then, between $z = a$ and $1 - a$, the radial

velocity is set to zero. Because Ψ is constant in this region, the azimuthal velocity is also constant. This constant azimuthal velocity, which is in general non-zero, is simply $v(r = 1, z = a)$.

The consistency condition at $r = 0$ is handled much like the $r = 1$ closed-end condition. The radial and azimuthal velocities are extrapolated back to $r = 0$ and, if the radial velocities do not vanish, the collision-region analysis is applied to determine a matching condition. At $r = 0$, however, the negative (incoming) radial velocities and their associated azimuthal velocities are left unchanged and the positive radial velocities adjusted to be antisymmetric about z_0, in contrast to the procedure at $r = 1$.

Because we do not need to resolve the details of the flow in the $O(H/L)$ region at $r = 1$, our numerical procedure is fast and efficient. Also, we are able to finely resolve the region near the axis of rotation, and thereby investigate the validity of the similarity solution as $r \to 0$.

3. Results

In this section, we shall present results at three different rotation ratios: $s = -1$, 0 and -0.8 as well as comparisons with experiment. Our results include velocity and pressure-gradient profiles. It is our aim to determine which, if any, of the similarity solutions describes the flow over a portion of the domain between finite rotating disks. Near the outer edge, the effect of the end will be important and the flow will not be of the similarity form. As the axis of rotation is approached, however, the effect of the end will generally decrease and the solution may approach similarity form. To concisely compare the finite-disk and similarity-solution results, we shall plot $1/r(\mathrm{d}p/\mathrm{d}r)$ evaluated at a single radial location for both solutions. This quantity, for either the finite disk or similarity solution, will be referred to as the pressure coefficient. Because we are interested in determining if the solutions agree anywhere in the flow domain and because we expect agreement, if it does exist, to occur near the axis of rotation, we choose to compare the pressure coefficients for the two solutions at $r = 0.1$. For both flows, $1/r(\mathrm{d}p/\mathrm{d}r)$ does not vary axially and for the similarity solution it is a constant, equal to $\beta/2Re$ (cf. $(1d)$). The pressure coefficient is representative of the finite-disk flow at a particular radial location and is therefore a useful variable for comparison.

For the similarity solution to be considered a 'valid' description of the flow between rotating disks at a given radial position, or for the two solutions to be considered to 'agree', we require that the pressure coefficients for the two solutions not vary by more than 2% at the specified radial location. This, we feel, is representative of the accuracy of our numerical solutions. Other flow properties were found to show comparable agreement, indicating that comparison of $1/r(\mathrm{d}p/\mathrm{d}r)$ is a valid approach. In some cases, the flow between finite rotating disks may resemble qualitatively, but not agree quantitatively with, the similarity solution. In these instances, we shall describe the finite-disk flow as 'resembling' the similarity solution and shall, in some cases, indicate the magnitude of the discrepancy.

For additional velocity and pressure-profile plots and further comparisons with the similarity solution see Durlofsky (1986).

3.1. *Exact counter-rotation: $s = -1$*

We first consider the case of exact counter-rotation, $s = -1$. A plot of the pressure coefficient, $\beta/2Re$, *vs.* Re is shown in figure 2; the solid curves are the similarity

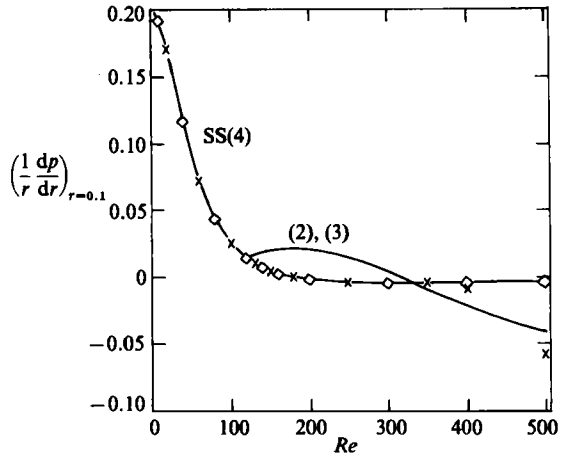

FIGURE 2. Comparison of the $s = -1$ pressure coefficients at $r = 0.1$ for similarity and finite-disk flows; ——, similarity solution; ◇, open-end flows; ×, closed-end flows. The numbering of the similarity solution on this and all subsequent figures corresponds to the numbering scheme of Szeto (1978). Branch 4 is the symmetric Stewartson solution. Branches 2 and 3 appear together in this representation.

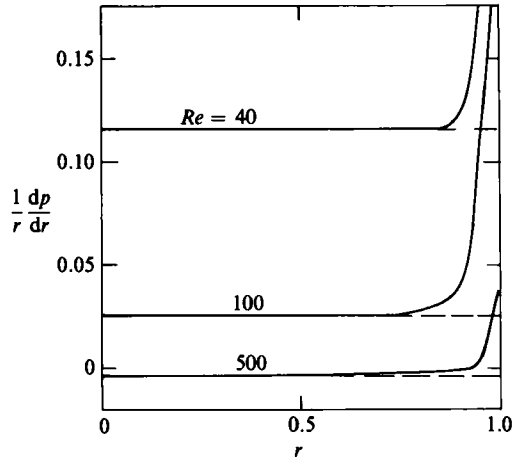

FIGURE 3. Pressure-gradient profiles for the $s = -1$ open-end finite-disk flows at $Re = 40$, 100 and 500. The dashed lines correspond to the pressure-gradient profiles of the Branch 4 similarity solution.

solutions. The one continuous solution (Branch 4 using Szeto's notation), which extends from 0 to ∞ in Re, is the symmetric solution; its radial velocities are symmetric about the midline $z = 0.5$, its angular velocities antisymmetric. At high Re ($Re > 200$) Branch 4 solutions are of the Stewartson type – both disks locally throw fluid out in the positive radial direction and, in the core, the returning radial velocity is $O(Re^{-\frac{1}{2}})$ in magnitude, while the angular velocity approaches zero outside the $O(Re^{-\frac{1}{2}})$ thin boundary layers located adjacent to each disk. At $Re = 119.8$, the solution bifurcates supercritically to two asymmetric solutions labelled Branches 2 and 3. (Only one new solution appears on figure 2 because the two asymmetric solutions have identical β-values. Had we plotted another solution variable such as the azimuthal velocity at the midline, $g(z = \frac{1}{2})$, the two solutions would be apparent.)

These asymmetric solutions are not of Stewartson type – at high Reynolds number they possess non-zero angular velocities in the core. Additional, non-Stewartson type solutions appear at $Re = 55$ and extend to $Re \to \infty$ but are not shown in figure 2 because their velocity fields are highly aphysical with angular velocities in the core very much greater in magnitude than that of the disks. Branch 4 similarity solutions are temporally stable up to the $Re = 119.8$ bifurcation; at the bifurcation they lose stability to the Branch 2 and 3 solutions.

We now turn to the flow between disks of finite radii, considering first the open end condition. Figure 3 is a plot of the pressure coefficient as a function of r at $Re = 40$, 100 and 500. The solid curves are the finite-disk results, the dashed lines the Branch 4 (symmetric) similarity solution. The influence of the end is evident near $r = 1$ where the pressure gradient deviates from the similarity solution, and this deviation is seen to propagate inward with increasing Reynolds number. At low Reynolds number ($Re = 10$), the end effect is important only for $0.92 < r \leqslant 1$; thus, throughout the bulk of the flow domain, $0 \leqslant r \leqslant 0.92$, the similarity solution is valid. (As mentioned above, by valid we mean that the similarity solution and the finite-disk solution agree at all axial locations at a given radial position with an error of at most 2 %). By $Re = 40$, the end effect propagates further inward to $r = 0.85$, and for $Re = 100$, to $r = 0.7$. Thus, we see that, at low to moderate values of the Reynolds number, the effect of the end increases noticeably with increasing Reynolds number. While appreciable over a large portion of the flow, the effect of the end at high Reynolds number changes slightly with increasing Reynolds number. At $Re = 300$, the similarity solution is valid only for $0 \leqslant r \leqslant 0.15$, but the discrepancy between pressure coefficients for the two solutions is still only 10 % at $r = 0.5$. At $Re = 500$, the similarity solution is valid over a comparable region, with a 14 % deviation at $r = 0.5$.

To concisely present the $s = -1$ open-end results, in figure 2 we compare $1/r(\mathrm{d}p/\mathrm{d}r)$ evaluated at a single point near the axis of rotation, $r = 0.1$, (diamonds) with the similarity solution. Near the axis of rotation the finite-disk open-end solutions agree with the symmetric similarity solution for all values of Re considered. Beyond $Re = 119.8$, then, we have an unusual result: the flow between finite rotating disks, over a region near the axis of rotation, is described by a temporally unstable similarity solution. Because our numerical solution procedure involves a time integration, we would expect to find only temporally stable steady solutions. It should be noted, however, that these finite-disk solutions were all calculated by incrementing the Reynolds number. Thus, the initial condition for each run was the symmetric $s = -1$ solution at the previous Reynolds number, so that each solution was subjected to only symmetric disturbances – all asymmetric disturbances were entirely suppressed by the iteration procedure for the end condition. We shall see that the introduction of an asymmetric disturbance will reconcile this apparent discrepancy.

Aside from the fact that the symmetric $s = -1$ similarity solution is temporally unstable at high Re, it is not surprising that the flow between finite rotating disks with an open end should decay to a Stewartson-like flow near the axis of rotation. The open-end boundary condition resembles closely a high-Re Stewartson solution – it has both disks dominating the flow locally, with a zero angular and uniform radial velocity core. The qualitative resemblance of the open-end condition to the symmetric similarity solutions is apparent in figure 4(a,b), where the radial and azimuthal velocity profiles at different values of r are plotted for $Re = 200$. Note the uniform radial velocity and zero azimuthal velocity of the incoming fluid at $r = 1$. These velocity profiles, like all $s = -1$, open-end velocity profiles that have not been

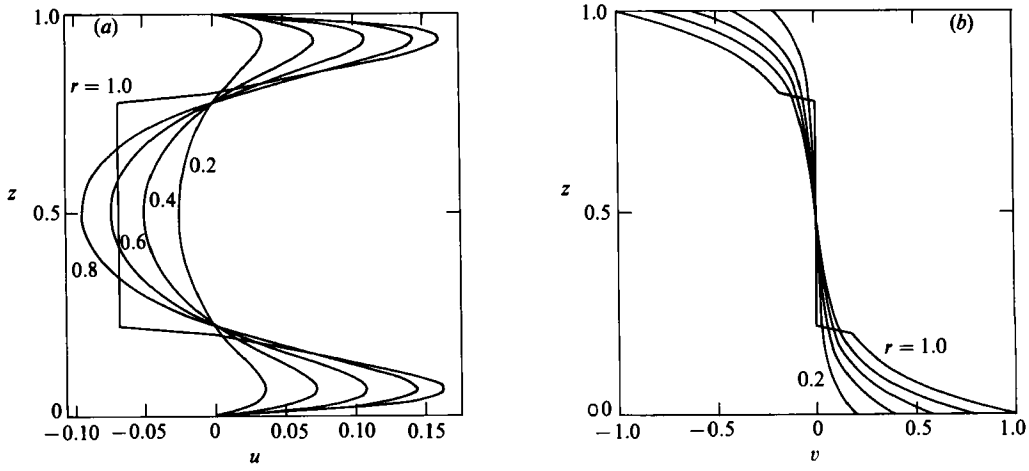

FIGURE 4. Velocity profiles for the $Re = 200$, $s = -1$ open-end flow at $r = 0.2, 0.4, 0.6, 0.8$ and 1.0: (*a*) radial velocities; (*b*) azimuthal velocities. Note the uniform radial velocity and zero azimuthal velocity of the incoming fluid at $r = 1$.

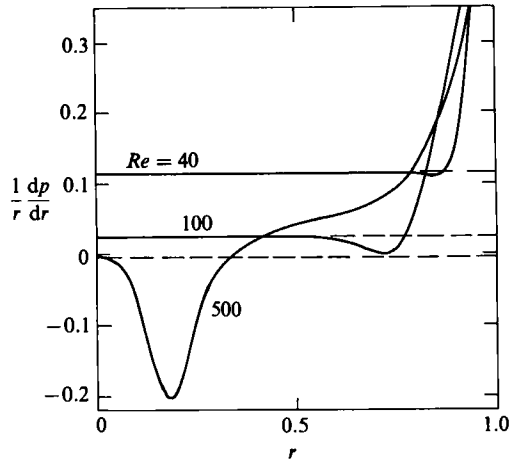

FIGURE 5. Pressure-gradient profiles for the $s = -1$ closed-end finite-disk flows at $Re = 40$, 100 and 500. The dashed lines correspond to the pressure-gradient profiles of the Branch 4 similarity solution. Note the presence of a collision region (non-zero slope as $r \to 0$ of the pressure coefficient) for the $Re = 500$ finite-disk flow.

subjected to asymmetric disturbances, are symmetric at all values of r. For $Re = 200$, however, they do not attain similarity form until $r = 0.3$.

We now turn to the $s = -1$ closed-end results. Figure 5 is a plot of the pressure coefficient versus r. As was the case for the $s = -1$ open-end flows, the end effect increases noticeably with increasing Reynolds number for low to moderate Reynolds numbers. At $Re = 40$, the similarity solution is valid for $0 \leqslant r \leqslant 0.8$ and at $Re = 100$ for $0 \leqslant r \leqslant 0.5$. By $Re = 250$, however, the two solutions agree only up to $r = 0.1$. This trend continues for the closed-end flows and, for $Re \geqslant 400$, the effect of the end has actually propagated all the way back to the axis of rotation, where a collision region appears at $r = 0$. The collision region is manifested by the non-constant $1/r(dp/dr)$ as $r \to 0$, which indicates that the similarity solution no longer provides

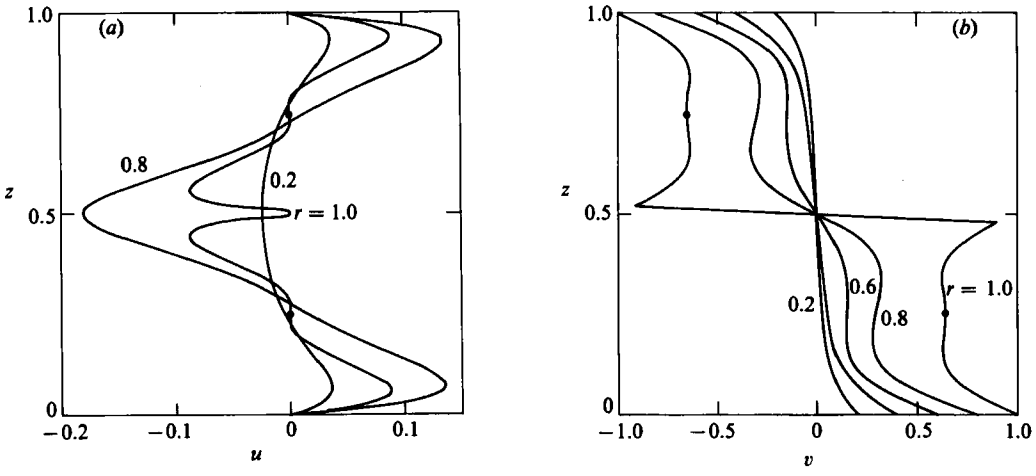

FIGURE 6. Velocity profiles for $Re = 200$, $s = -1$ closed-end flow: (*a*) radial velocities at $r = 0.2$, 0.8 and 1.0; (*b*) azimuthal velocities at $r = 0.2, 0.4, 0.6, 0.8$ and 1.0. The circles correspond to z_0 – the points about which the radial velocity is antisymmetric and the azimuthal velocity symmetric.

a valid description of the flow over any portion, no matter how small, of the flow domain. The reason for the appearance of the $r = 0$ collision region at high Re will be discussed below.

The crosses in figure 2 summarize the $s = -1$ closed-end results. As for the open-end flows, they represent $1/r(\mathrm{d}p/\mathrm{d}r)$ evaluated at $r = 0.1$. For $Re \leqslant 350$, the closed-end solutions decay into the symmetric, temporally unstable, similarity solution. This is really quite surprising because the $r = 1$ closed-end boundary condition, though symmetric, does not resemble the symmetric, Stewartson-like similarity solution. This is apparent from figure 6 (*a*, *b*) where the closed-end radial and azimuthal velocity profiles are plotted for various values of r for $Re = 200$. The points marked with circles on the $r = 1$ profiles correspond to z_0 – the axial location where the radial velocity is zero and about which the radial velocity is antisymmetric and the azimuthal velocity symmetric. The discontinuities in the velocity fields at $r = 1$, $z = 0.5$ are allowable because, to a first approximation, the flow is inviscid at $r = 1$.

The $Re = 500$, closed-end point on figure 2 appears near the Branch 2 and 3 similarity solution but it does not resemble either of these solutions. Though not of similarity form, the $Re = 500$ closed-end solution is symmetric about the midline at all radial locations except near the $r = 0$ collision region. Over the region $0 \leqslant r \leqslant 0.5$ its velocity profiles most resemble the Branch 4 similarity solution, but precise agreement is never attained.

Comparing figure 6 (*a*) with figure 4 (*a*), we see a noticeable difference between the decay of the two radial velocity profiles into the similarity solution. By $r = 0.8$, for the closed-end solution, the two returning jets of fluid, clearly visible at $r = 1$, have merged into one. The momentum of the returning radial velocity, therefore, is considerably larger at $r = 0.8$ for the closed-end solution than for the open-end solution. For $Re \geqslant 400$, the radial velocity in the closed-end flows does not decay into the similarity solution by $r = 0$, and a collision region forms at the axis of rotation. At high Re, the flow in the core does not have sufficient viscosity to damp the returning jet of fluid and so a collision region forms.

The differences in the details of the flow fields between the $s = -1$ similarity

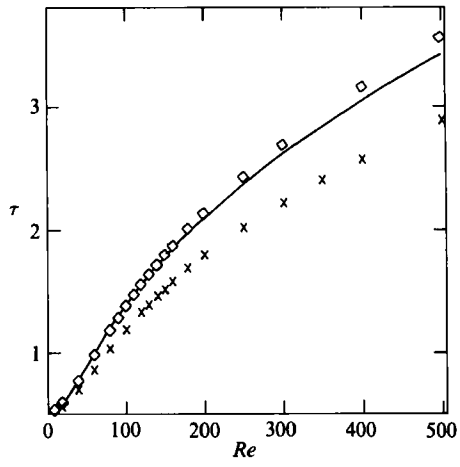

FIGURE 7. Dimensionless torque on either disk for the $s = -1$ flows. ——, similarity solution; ◇, open-end flows; ×, closed-end flows.

solution and the finite-disk solutions do not necessarily imply major differences in global quantities. For example, let us consider the total torque exerted by the fluid on the top disk, defined as

$$\tau = \frac{T_z}{2\pi\mu\Omega L^4/H} = -\int_0^1 \frac{\partial v}{\partial z}(r,1)\, r^2 \mathrm{d}r. \tag{11}$$

Figure 7 shows a plot of the dimensionless torque as a function of Re for the similarity solution and the open- and closed-end finite-disk solutions. Because these flows are all symmetric, the magnitude of the torque is the same at both disks. As we might expect, the torques for the open-end flows are closer to the similarity solution than are those of the closed end. At $Re = 200$, the open-end finite-disk solution agrees with the similarity solution only for $0 \leqslant r < 0.3$, yet the torques are nearly identical. This is because the torque only depends on the axial derivative of the azimuthal velocity at the disk surface; the details of the flow away from the disk are of little importance. Even though the $s = -1$ open-end flow does not resemble the similarity solution at all axial locations for $r > 0.3$, the flow in the immediate vicinity of the disks – within the boundary layers – is quite close to the similarity solution for all r. Note that the closed-end finite-disk torques fall below those of the similarity solution. For the similarity solution, the azimuthal velocity quickly decays to zero away from the disks, but for the closed-end finite-disk flows, the azimuthal velocity decays less rapidly near the disk and displays a sizeable gradient at the midline, as is apparent from figure 6(*b*). Thus, owing to the smaller gradient in azimuthal velocity near the disk surface, the closed-end finite-disk torques are less than those of the similarity solution.

We have seen that, for all the $s = -1$ finite-disk open-end flows and for the closed-end flows below a Reynolds number of 400, the solution returns to the Branch 4 symmetric similarity solution near the axis of rotation. For $Re > 119.8$, however, this similarity solution is temporally unstable. In our numerical scheme when proceeding from one Reynolds number to another, we have applied a purely symmetric disturbance to the system. Physically, this corresponds to increasing the magnitude of the rotation rates of both disks by precisely the same amount

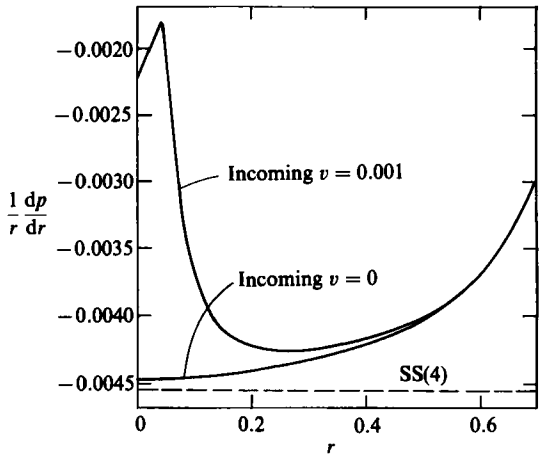

FIGURE 8. Pressure gradient profiles for the $Re = 300$, $s = -1$ open-end finite-disk flows with zero and 0.001 incoming azimuthal velocity. The dashed line corresponds to the Branch 4 similarity solution. The non-zero incoming azimuthal velocity results in a collision region, while the zero case is of similarity form near $r = 0$. The slight discrepancy between the zero incoming azimuthal velocity flow and the similarity solutions is less than the accuracy of the computations, i.e. less than 2%.

simultaneously. To consider the effects of asymmetry, disturbances that were asymmetric about the midline $z = 0.5$ were applied at the end $r = 1$ to the symmetric, steady, both open- and closed-end flows over a range of Reynolds number. Above $Re \approx 140$ for the open-end solutions and $Re \approx 120$ for the closed-end solutions, the introduction of asymmetry into the flow results in a subtle though fundamental change in the solution structure: a collision region forms at $r = 0$, nullifying the similarity solution as a valid description of the flow near the axis of rotation. This is apparent by reference to figure 8 where we plot $1/r(\mathrm{d}p/\mathrm{d}r)$ versus r at $Re = 300$ for three different steady solutions: the Branch 4 similarity solution (horizontal dashed line); the open-end finite-disk solution without the application of an asymmetric disturbance; and the open-end solution with the angular velocity of the incoming fluid set to 0.001 rather than zero. This slight deviation from zero for the incoming angular velocity represents a small-amplitude asymmetric disturbance to the Branch 4 similarity solution; this angular velocity does *not* correspond to the angular velocity of the asymmetric Branch 3 similarity solution, which, at $Re = 300$, has $g(\frac{1}{2})$ equal to 0.407. The finite-disk solution without the disturbance is of similarity form near the axis of rotation ($0 \leqslant r \leqslant 0.15$). The slight discrepancy in this region between it and the similarity solution, apparent in figure 8 because of the enlarged scale, is less than 2%. The solution with the asymmetric disturbance is indistinguishable from that without for $0.5 \leqslant r \leqslant 0.95$ (there is of course a small discrepancy near the end $r = 1$), where neither agrees with the similarity solution. At $r = 0.2$, the discrepancy in the pressure coefficients between the two finite-disk solutions is still only 4%, but, as $r \to 0$, where the finite-disk solution without the asymmetric disturbance becomes of similarity form, the $s = -1$ open-end solution with non-zero incoming angular velocity diverges abruptly, forming a collision region at the axis of rotation. Thus, it is not of similarity form anywhere in the flow domain.

It is apparent from our numerical simulations that some type of asymmetry must be introduced into the system to cause a collision region to form near the axis of

rotation and thus negate the similarity solution as a valid description of the flow between finite rotating disks as $r \to 0$. In any experimental system, some asymmetry will always be present and our numerical results suggest that a collision region will form. The collision region might be difficult to observe experimentally, however, because its actual size is only $O(H/L)$ and the velocities, although not zero, are nonetheless small. Note that even though asymmetry has been introduced and the similarity solution is not valid as $r \to 0$, or anywhere else in the flow domain, the finite-disk solution *does not* approach the stable asymmetric similarity solution at these Reynolds numbers. Indeed, there is still a region in r over which the finite-disk solution qualitatively resembles the unstable symmetric similarity solution.

To understand why the $s = -1$ finite-disk solution retains Branch 4 similarity form when subjected to symmetric disturbances but not when subjected to asymmetric disturbances, we consider the linearized temporal stability of the similarity solution. A temporal stability analysis of the Branch 4 $s = -1$ similarity solution reveals the existence of a single positive (growing in time) eigenvalue for $Re > 119.8$. The eigenfunction corresponding to this unstable eigenvalue has a radial velocity component that is antisymmetric about $z = 0.5$ and an azimuthal velocity component that is symmetric. At any particular Reynolds number the difference between the $s = -1$ finite-disk end condition and the similarity solution can be expressed in terms of the orthonormal eigenfunctions of the Branch 4 similarity solution, i.e.

$$u(r = 1, z) + \tfrac{1}{2} f'(z) = \sum_{n=1}^{N} a_n P_n(z), \tag{12a}$$

$$v(r = 1, z) - g(z) = \sum_{n=1}^{N} d_n Q_n(z), \tag{12b}$$

where f' and g are the similarity functions, $\{P_n, Q_n\}$ are the eigenfunctions, $\{a_n, d_n\}$ are the amplitude coefficients and N is the total number of modes. The unstable mode is designated by $n = 1$. Recall that $f'(z)$ is symmetric about $z = 0.5$ and $g(z)$ antisymmetric. If we now consider various end conditions, we conclude that, if $u(r = 1, z)$ is symmetric about $z = 0.5$ then, because $P_1(z)$ is antisymmetric, the amplitude coefficient for the unstable mode a_1 is identically zero. Similarly, if $v(r = 1, z)$ is antisymmetric, then, because $Q_1(z)$ is symmetric, $d_1 = 0$. Both the $s = -1$ open- and closed-end conditions have u symmetric and v antisymmetric about $z = 0.5$ (cf. figures 4*a*,*b* and 6*a*,*b*) in accordance with the asymptotic turning-region analysis. Thus, the two end conditions that we have considered, due to their symmetries, do not excite the unstable mode. End conditions that lack these symmetries will, in general, excite the unstable mode.

Different types of asymmetric disturbances affect the steady, undisturbed solutions in the same qualitative way. For the open-end flows, non-zero incoming angular velocity, for $Re \geqslant 140$, results in the formation of a collision region near the axis of rotation, negating the similarity solution as a valid description of the flow anywhere in the flow domain. For closed-end flows, positioning the returning jets of fluid asymmetrically about $z = 0.5$ has a similar effect.

Both of the above disturbances were applied continuously at the end $r = 1$. Instantaneous disturbances were also applied to the steady solutions. These disturbances generally involved small-amplitude, mass-conserving perturbations to the radial velocity profile at all radial locations. After an initial transient period of dimensionless time 30 or 40, in most cases such disturbances did not have as great an effect on the flow as did the continuous $r = 1$ disturbances. It is not entirely clear

whether the instantaneous disturbances would ultimately decay completely or would persist, invalidating the similarity solution near the axis of rotation. This seems to be dependent on the type and amplitude of the instantaneous disturbance, as well as the Reynolds number of the flow.

In the open-end runs with non-zero incoming angular velocities referred to above, the incoming angular velocity deviated only slightly from the zero centreline angular velocity of the Branch 4 symmetric similarity solution. When the angular velocity of the incoming fluid is set to correspond to the centreline angular velocity of one of the *asymmetric* similarity solutions, however, the finite-disk flow resembles the *asymmetric* similarity solution over a portion of the flow domain. This was observed both at $Re = 140$, where the pressure coefficient for the finite disk and asymmetric similarity solution deviate by less than 25 % for $0 \leqslant r < 0.5$, and at $Re = 200$, where deviation of less than 25 % in pressure coefficient exists for $0 \leqslant r < 0.2$. This type of end condition corresponds to a realizable experimental configuration in which the unbounded fluid surrounding the disks is rotated. So, simply by rotating the fluid in which the disks are immersed, an experimentalist can affect which similarity solution the flow will resemble far removed from the end. This result emphasizes the effect of the end condition (and specifically the angular velocity) in determining which similarity solution the finite-disk flow resembles. We shall see this phenomenon again in the $s = 0$ flows.

For both the open- and closed-end $s = -1$ flows, we find the solution to be unique at all values of Reynolds number considered. (The effects of the uncertainty about the location of z_0 are confined to within several grid points of $r = 1$ and, if the returning streams are located such that their positions are asymmetric about $z = 0.5$ and a collision region forms at $r = 0$, to within several grid points of $r = 0$. The solution over the bulk of the domain is, however, essentially unaffected.) This is in contrast to the results of Harriott & Brown (1984) who found multiple solutions at $s = -1$ for flow in a non-deformable cylindrical drop at aspect ratios up to three. At an aspect ratio of three, however, their asymmetric solutions were not asymmetric over the entire flow domian; at $Re = 67$ (Re here is based solely on the gap width H) the asymmetry was confined to $0.3 \leqslant r \leqslant 1$. At an aspect ratio of one, by contrast, the asymmetry extended over the entire flow domain, but nowhere resembled any of the asymmetric similarity solutions. These results, interpreted in the light of the solution uniqueness we observe, suggest that any solution multiplicity that may be observed at intermediate to large aspect ratios will be confined to an $O(H/L)$ region near $r = 1$ and possibly, if a collision region develops, to an $O(H/L)$ region near $r = 0$. Because we do not resolve the details of the $O(H/L)$ region near $r = 1$, we observe solution uniqueness. This also explains why Harriott & Brown found a larger region of asymmetry at an aspect ratio of one than at an aspect ratio of three.

In summary, we have seen that the $s = -1$ open-end flows return to the Branch 4 symmetric similarity solution as $r \to 0$ for all Reynolds numbers considered. The closed-end flows return to the Branch 4 solution for Reynolds number below 400; for $Re \geqslant 400$, a collision region forms at the axis of rotation and the flow does not resemble any similarity solution. The application of a continuous asymmetric disturbance causes the formation of a collision region at $r = 0$ for $Re > 140$ for flows with either type of end condition, thus invalidating the similarity solution as $r \to 0$.

3.2. *One rotating and one stationary disk: $s = 0$*

We next consider the case of one disk rotating and the other stationary: $s = 0$. A plot of $\beta/2Re$ *vs.* Re is shown in figure 9; the solid curves again represent the similarity

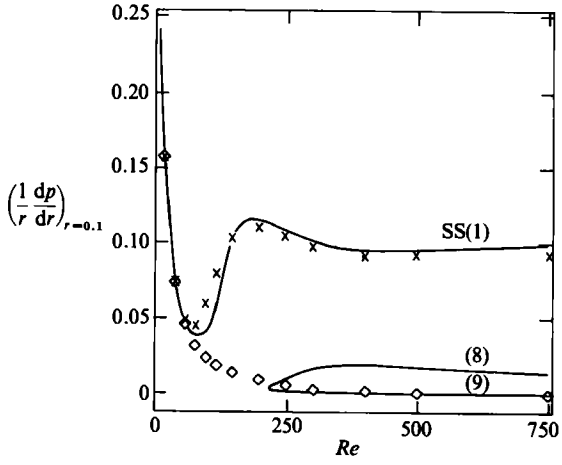

FIGURE 9. Comparison of the $s = 0$ pressure coefficients at $r = 0.1$ for similarity and finite-disk flows: ——, similarity solution; ◇, open-end flows; ×, closed-end flows. Branch 1 is the Batchelor solution and Branch 9 the Stewartson solution.

solution. Only three of the many existing solution branches are shown; the others possess rather aphysical velocity profiles. Branch 1 (again with the numbering scheme of Szeto), which extends from 0 to ∞ in Re, is the one-cell Batchelor solution. At high Re, these solutions display significant velocity gradients near both disks. Two new one-cell solutions, Branches 8 and 9, appear at $Re = 216.9$. At high Re, Branch 8 solutions display non-uniform radial velocity profiles and constant but negative angular velocities in the core. Branch 9 solutions are Stewartson solutions. At high Re, these solutions approach the von Kármán free-disk solution; they possess an $O(Re^{-\frac{1}{2}})$ thick boundary layer of fluid thrown radially outward and a negative, $O(Re^{-\frac{1}{2}})$ in magnitude, radial velocity in the core. The angular velocity approaches zero beyond the $O(Re^{-\frac{1}{2}})$ boundary layer, but there is a small overshoot, resulting in slightly negative angular velocities in the core. Branch 1 and Branch 8 solutions are temporally stable and Branch 9 solutions temporally unstable.

We now consider the $s = 0$ finite-disk results. A comparison between the similarity solution and the open-end, finite-disk solution is shown in figure 9 where we plot $1/r(dp/dr)$ evaluated at $r = 0.1$, respresented as diamonds. Near the axis of rotation, for Re up to about 60, the open-end finite-disk results agree with the Branch 1 similarity solution (i.e. the two solutions vary by less than 2%). At $Re = 40$, the two solutions agree for $0 \leqslant r \leqslant 0.35$. At $Re = 80$, the two solutions do not agree at $r = 0.1$, as is apparent from figure 9, but they do agree asymptotically as $r \to 0$. For $80 < Re \leqslant 250$, the effect of the end propagates all the way back to the axis of rotation, and there is no longer agreement with any similarity solution. A collision region at $r = 0$ appears for these flows for $Re > 200$. Above $Re \approx 250$, the open-end finite-disk flows take on a Stewartson form, and the solutions resemble the temporally unstable Branch 9 similarity solution at moderate values of r. These finite-disk solutions, however, have a collision region at $r = 0$, and therefore are not of similarity form as $r \to 0$. As was the case for the $s = -1$ solutions beyond $Re = 120$ after the application of an asymmetric disturbance, we again see that the flow between disks of finite extent resembles a temporally unstable similarity solution over part of the flow domain but forms a collision region near the axis of rotation. For the $s = 0$

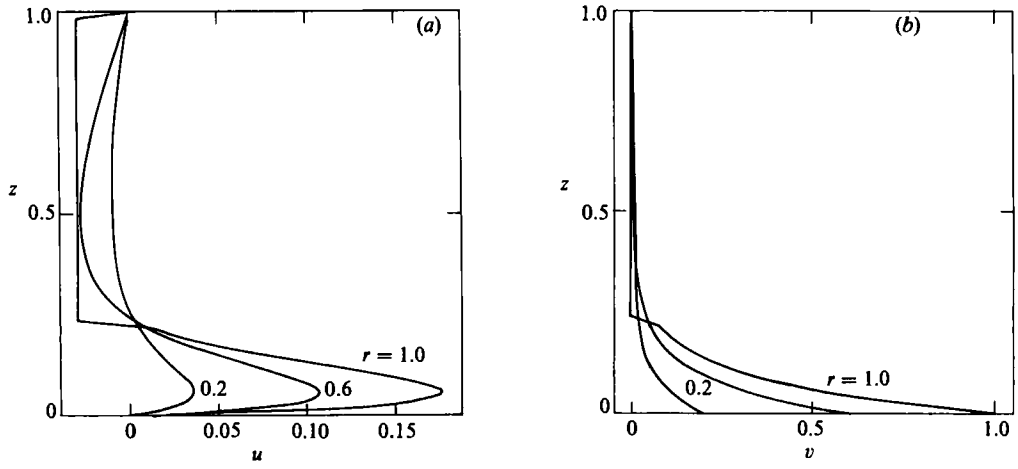

FIGURE 10. Velocity profiles at $r = 0.2$, 0.6 and 1.0 for the $Re = 250$, $s = 0$ open-end flow: (*a*) radial velocities; (*b*) azimuthal velocities.

open-end flows, however, the $r = 1$ end condition excites the unstable mode, and the application of an additional disturbance is not necessary.

The resemblance between the $s = 0$ open-end finite-disk flows and the $s = 0$ Branch 9 similarity solution is, for $Re \geqslant 250$, quite close in the range $0.3 < r < 0.6$, though again we stress that quantitative agreement is never attained. For example, at $Re = 500$, the pressure coefficient for the finite-disk flow deviates from that for the similarity solution by only 7% at $r = 0.5$, though it differs by almost 100% at $r = 0.2$ and by 30% at $r = 0.7$. Also, the open-end flows never display negative centreline angular velocities, though the Branch 9 similarity solutions do (e.g. for $Re = 500$, $g(\frac{1}{2}) = -0.00275$).

Radial and azimuthal velocity profiles are shown in figure 10(*a*,*b*) at $Re = 250$ for $s = 0$ open-end flow; both are reminiscent of the Branch 9 similarity solution over the entire domain. Even the $r = 1$ end condition – zero angular velocity and uniform radial velocity of the incoming fluid – is close to the Branch 9 similarity solution. The Stewartson form of this flow is very apparent; the azimuthal velocity quickly decays to zero away from the rotating disk and the inward-flowing radial velocity is nearly constant. No appreciable gradients in either the radial or azimuthal velocity exist near the top disk for any value of r. We shall see that the situation is much different for the closed-end condition.

The closed-end $s = 0$ results, represented by crosses, are summarized in figure 9. Here again we see agreement with the Branch 1 similarity solutions, for small r, up until $Re \approx 60$. For $Re = 40$, the two solutions agree for $0 \leqslant r \leqslant 0.2$. At $Re = 80$, the two solutions do not agree at $r = 0.1$, but, as was the case for the open-end flows, they do agree asymptotically as $r \to 0$.

For larger Re, $80 < Re \leqslant 150$, however, the two solutions do not agree anywhere in the flow domain, but no collision region develops at the axis of rotation. In this range, the solutions differ only slightly near the axis of rotation. For example, at $Re = 100$, the pressure coefficients for the two solutions differ by only 8% at $r = 0.02$. For $200 \leqslant Re \leqslant 1000$ (solutions for $Re > 750$ are not shown in figure 9), the two solutions agree asymptotically for some values of Reynolds number as $r \to 0$, but differ

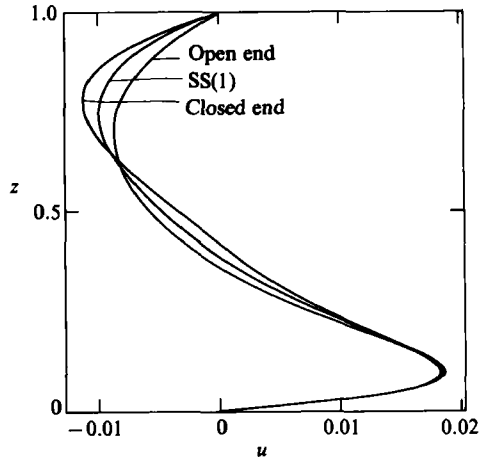

FIGURE 11. Radial velocity profiles for $Re = 100$, $s = 0$ for open-end, closed-end and similarity flows at $r = 0.1$. The discrepancies between the three solutions persist as $r \to 0$.

over the bulk of the flow domain. Again, however, no collision region develops at the axis of rotation. At $Re = 200$, the pressure coefficients for the two solutions agree only at the axis of rotation, differ by 4% at $r = 0.1$ and by 24% at $r = 0.6$. At $Re = 500$, the solutions differ by 3% at the axis of rotation, by 4% at $r = 0.1$ and by 50% at $r = 0.6$. Thus, we can state generally that beyond $Re = 80$, the closed-end $s = 0$ flows resemble the Branch 1 similarity solution over a portion of the domain near $r = 0$, but quantitative agreement, if it exists at all, is limited to an extremely small (< 0.04) region near the axis of rotation. Similar behaviour was observed by Dijkstra & van Heijst (1983) at an aspect ratio of 14. Their $Re = 1000$, $s = 0$ velocity profiles resembled, but did not precisely agree with, the Branch 1 similarity solution at the lowest non-zero r ($r = 0.2233$) their mesh contained, though the quantitative discrepancy at this radial location in, for example, axial velocity is at most about 7%, which may be due to grid resolution.

We can see the slight discrepancy between the finite-disk results and the Branch 1 similarity solution at moderate Reynolds number by reference to figure 11 where we plot the radial velocity profiles at $r = 0.1$ and $Re = 100$ for the similarity solution and the open- and closed-end $s = 0$ flows. Both the finite-disk solutions are already tending towards their high-Re asymptotic behaviour: the closed-end profile displays larger gradients near the top disk than either the similarity solution or the open-end flow. These differences between the finite-disk results and the similarity solution persist as $r \to 0$.

Figure 12(a,b) depicts radial and angular velocity profiles for $Re = 250$, $s = 0$ closed-end flow. The Batchelor form of these velocity fields is apparent – significant axial gradients exist in both the radial and azimuthal velocities near both disks and the core flow possesses a constant but non-zero angular velocity. By $r = 0.2$, both the radial and azimuthal velocity profiles resemble the similarity solution, but they do not agree quantitatively. The two solutions do agree asymptotically as $r \to 0$. The radial velocity profile at $r = 1$ shown in figure 12(a) shows the fluid being thrown out as a jet by the bottom disk, traversing up the disk enclosure and returning as a jet adjacent to the top disk. The end condition for the radial velocity qualitatively resembles the Branch 1 similarity solution at high Re. The end condition for the

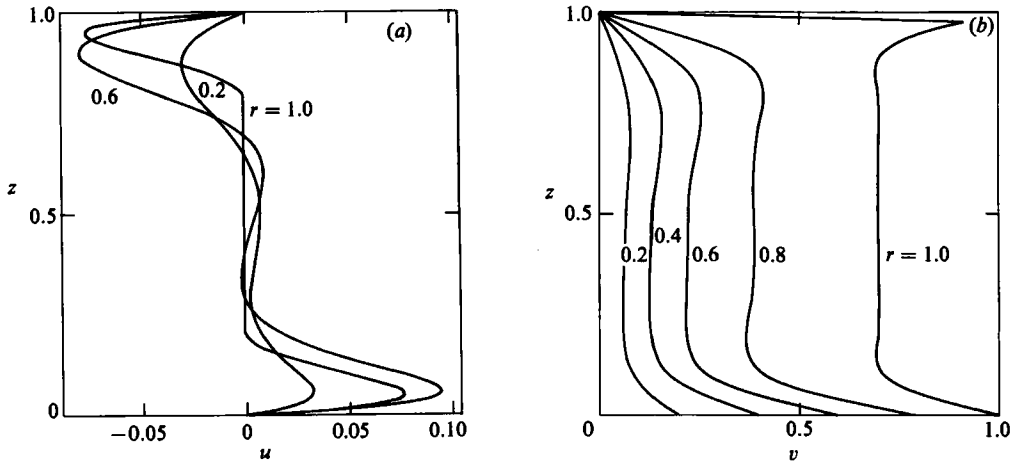

FIGURE 12. Velocity profiles for the $Re = 250$, $s = 0$ closed-end flow: (*a*) radial velocities at $r = 0.2$, 0.6 and 1.0; (*b*) azimuthal velocities at $r = 0.2$, 0.4, 0.6, 0.8 and 1.0.

azimuthal velocity, shown in figure 12(*b*), however, does not resemble the similarity solution. The angular velocity in the core is 0.7 compared with 0.35 for the Branch 1 similarity solution and, above the midline, the angular velocity continually increases rather than decreases as it approaches the top disk, with the appearance of a boundary layer at the top disk where the no-slip boundary condition is satisfied. (This boundary layer is $O[\{Re(L/H)\}^{-\frac{1}{2}}]$ in thickness, is inside the inviscid turning region and, for numerical purposes, we have simply left a discontinuity at the first axial grid point.) These qualitative and quantitative differences in the azimuthal velocity at $r = 1$ are sufficient to invalidate the similarity solution as a description of the flow over the bulk of the domain at high Re.

In summary, we see that the $s = 0$ flows return to the Branch 1 similarity solution as $r \to 0$ for $Re \leqslant 80$ regardless of the end condition. For $80 < Re \leqslant 150$, the closed-end flows resemble but do not agree with the Branch 1 Batchelor-type solution anywhere in the flow domain. At larger Re, $200 \leqslant Re \leqslant 1000$, some of the closed-end flows do agree with the Branch 1 similarity solution, but only in a very small region near the axis of rotation ($r < 0.04$). The open-end flows resemble no similarity solution for $80 < Re \leqslant 250$ but, for $Re > 250$, they do resemble the Branch 9 Stewartson-type one for small but non-zero r. These solutions vary from the similarity solution near the axis of rotation owing to the presence of a collision region at $r = 0$. Thus, we see again the profound influence that the end condition, and in particular the angular velocity, has on the flow throughout the entire domain between the two finite disks.

3.3. *Strong counter-rotation: $s = -0.8$*

We next briefly consider strong counter-rotation, $s = -0.8$, as it is qualitatively similar to exact counter-rotation, $s = -1$. Three of the many similarity solution families for $s = -0.8$ are shown in figure 13. The super-critical bifurcation, which occurs for the perfect case of exact counter-rotation, is ruptured; the resulting limit point for the Branch 3 and 4 solutions occurs at $Re = 158$. All three similarity solutions shown are two-cell solutions. At high Reynolds number, the Branch 2 solution displays a non-constant and negative angular velocity in the core and a maximum in radial velocity near the top (slower moving) disk. Branch 3 solutions

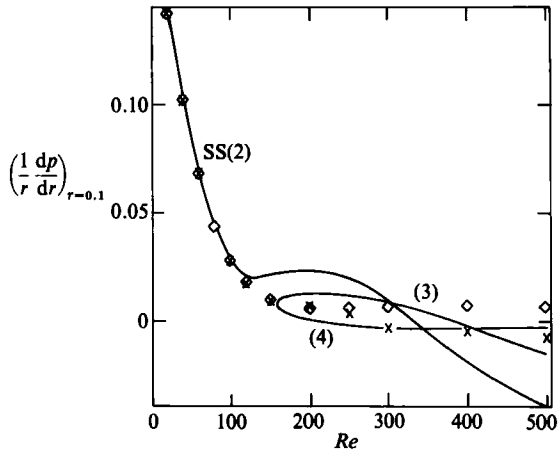

FIGURE 13. Comparison of the $s = -0.8$ pressure coefficients at $r = 0.1$ for similarity and finite-disk flows: ——, similarity solution; ◇, open-end flows; ×, closed-end flows. Branch 4 is the Stewartson solution.

are just the opposite, with a positive angular velocity in the core and a maximum in radial velocity near the bottom disk. Branch 4 solutions are agin of Stewartson-type; they are characterized by zero-angular-velocity cores and a maximum in radial velocity near the bottom disk. Branch 2 and 3 solutions are temporally stable, Branch 4 solutions unstable.

The finite-disk solutions are summarized in figure 13. Again, the diamonds represent $1/r(dp/dr)$ evaluated at $r = 0.1$ for the open-end solutions. At low to moderate Re ($0 < Re \leqslant 100$), the open-end flows agree with the Branch 2 similarity solution over a large portion of the flow domain. At $Re = 40$, the two solutions agree for $0 \leqslant r \leqslant 0.85$, and at $Re = 100$ they agree for $0 \leqslant r \leqslant 0.5$. For $Re > 120$, the open-end finite-disk solutions do not follow the Branch 2 similarity solution; instead, they tend toward the Branch 4 solution. At high Reynolds number ($200 \leqslant Re \leqslant 500$), however, the open-end flows do not appear to resemble any similarity solution at $r = 0.1$. This is in contrast to the $s = -1$ open-end flows, which, at $r = 0.1$ and in the absence of an asymmetric disturbance, coincide precisely with the Branch 4 similarity solution at all Re considered.

The $s = -0.8$ open-end flows do, at high Re, resemble the Branch 4 similarity solution over a portion of the flow domain. If we plot $1/r(dp/dr)$ evaluated at $r = 0.3$ (not shown), for example, the open-end points fall much closer to the Branch 4 curve at high Re. At $r = 0.3$ the pressure coefficient differs by only 17 % at $Re = 300$ and by 11 % at $Re = 500$ from the Branch 4 similarity solution. Near the axis of rotation, however, the solution deviates markedly from this Stewartson-type similarity solution, as was the case for $s = -1$.

A more careful look at the $s = -0.8$ open-end solutions at high Reynolds number reveals that the flow is actually described by two different similarity solutions in two different regions of the flow domain. Near $r = 1$, the effect of the end is important and the solution does not resemble any similarity solution. In an intermediate region ($0.2 \leqslant r \leqslant 0.4$) the finite-disk open-end flow resembles the Branch 4 similarity solution, as shown in figure 14(*a*), where we plot the radial velocity at $r = 0.3$ for the open-end finite-disk flow and the Branch 4 similarity solution. The symmetry of the finite-disk flow is apparent. This similarity solution is, however, temporally

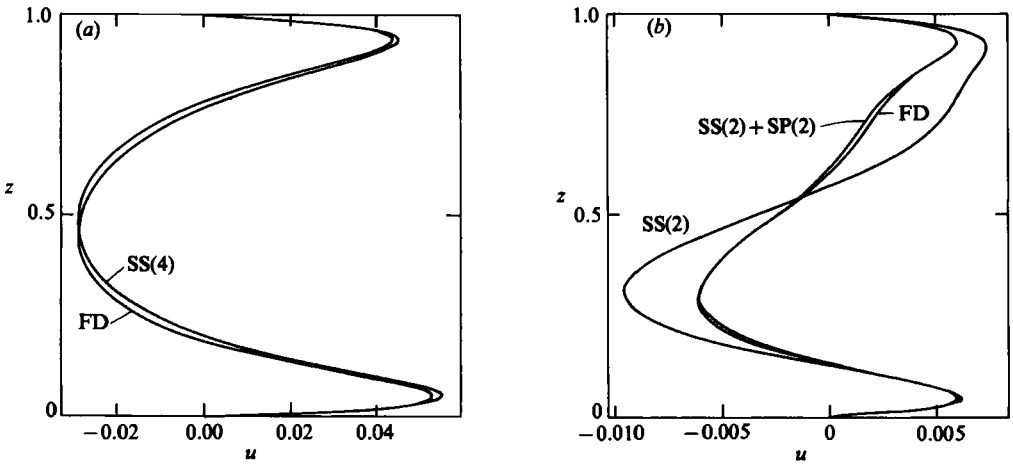

FIGURE 14. Comparison of $Re = 300$, $s = -0.8$ radial velocity profiles for open-end and similarity flows: (*a*) Branch 4 similarity solution and finite-disk solution at $r = 0.3$; (*b*) Branch 2 similarity solution, Branch 2 similarity solution plus small perturbation term, and finite disk open end solution at $r = 0.04$.

unstable. For $s = -1$, a collision region develops at $r = 0$ after the application of an asymmetric disturbance. For $s = -0.8$, a collision region develops as well, but a more fundamental change in the solution occurs – the Branch 2 similarity solution, plus a correction term associated with the Branch 2 solution, describe the flow near the axis of rotation, $0.02 \leqslant r < 0.1$.

This correction term is determined by a small perturbation analysis of the similarity solution, where solutions to the boundary-layer-like equations (4) of the form

$$u = -\tfrac{1}{2} r f'(z) - \sum_{n=1}^{\infty} k_n r^{\lambda_n} b_n'(z), \tag{13a}$$

$$v = r g(z) + \sum_{n=1}^{\infty} l_n r^{\lambda_n} c_n(z), \tag{13b}$$

etc. were sought. Here $\{\lambda_n\}$ and $\{b_n, c_n\}$ are eigenvalues and corresponding eigenfunctions and $\{k_n, l_n\}$ are amplitude coefficients. Such an analysis was performed by Durlofsky & Brady (1984) in their study of the similarity solutions describing flow in an infinite channel or tube with either porous walls or an accelerating surface velocity, as well as by Chen & Libby (1968) in their analysis of the Falkner–Skan equation for the boundary-layer flow over a wedge. The results of the analysis of Durlofsky & Brady were found to be useful in explaining discrepancies between the similarity solution and its finite-domain counterpart. Here too the small perturbation analysis is able to resolve the difference between the $s = -0.8$ finite-disk solution and the Branch 2 similarity solution. The $s = -0.8$, open-end solution at, for example, $Re = 300$, does not appear to resemble the Branch 2 similarity solution near the axis of rotation (cf. figure 13). However, the inclusion of the first eigenfunction, for which, at $Re = 300$, $\lambda = 1.67$, with an amplitude of -1, resolves this difference and demonstrates that the Branch 2 similarity solution, along with its small perturbation term, does indeed describe the flow between finite disks near the axis of rotation. This is apparent from figure 14(*b*) which shows the open-end finite-disk radial velocity profile at $r = 0.04$ as well as the Branch 2 similarity solution radial velocity both with

and without its small perturbation term. The need for the inclusion of the small perturbation term is apparent, as is the asymmetry which has developed between $r = 0.3$ and 0.04. Thus, near the axis of rotation, the open-end finite-disk flow is described by a non-Stewartson-type similarity solution, but elsewhere it is of Stewartson form.

For the flows described by the Branch 2 similarity solution and its small perturbation term, the collision region at the origin results from our extrapolation procedure. Because the amplitude coefficient associated with the small perturbation term is $O(1)$, we are linearly extrapolating a function that is not linear near $r = 0$ (recall that $\lambda = 1.67$) and this results in the appearance of a collision region. We note that an $O(1)$ amplitude coefficient is not inconsistent with the small perturbation analysis provided r is small and $\lambda > 1$, as is the case here. For further details on the small perturbation analysis, see Durlofsky (1986).

No other $s = -0.8$ open-end velocity profiles are shown; they are quite similar in form to the $s = -1$ open-end velocity profiles (figure 4*a*,*b*).

The closed-end finite-disk solutions are represented in figure 13 by the crosses. Qualitatively, they are similar to the open-end results. Near the axis of rotation, the closed-end flows resemble the Branch 2 similarity solution for $Re < 120$. At $Re = 40$, the two solutions agree for $0 \leqslant r \leqslant 0.08$ and at $Re = 100$ for $0 \leqslant r \leqslant 0.15$. Beyond $Re \approx 120$, the flows are not described by any similarity solution near the axis of rotation. Our numerical procedure failed to reach a steady state for $Re \geqslant 300$. The unsteadiness occurred primarily near the outer edge. The solution was steady, however, for $r < 0.6$, so we present the $1/r(\mathrm{d}p/\mathrm{d}r)$ results for $Re \geqslant 300$.

As was the case for the $s = -0.8$ open-end flows, the closed-end flows do resemble the Branch 4 similarity solutions at high Re over a portion of the flow domain, but deviate near $r = 0$. The solution as $r \to 0$ does not, in this case, agree with another similarity solution, as it did for the open-end flows. For the closed-end solutions, a collision region forms at $r = 0$, much like that which forms for the $s = -1$ closed-end flows (which were not subjected to an asymmetric disturbance) for $Re \geqslant 400$. For $s = -0.8$, however, this collision region appears at $Re \approx 200$. The $s = -0.8$ closed-end velocity profiles appear somewhat like their $s = -1$ counterparts. They resemble the Branch 4 Stewartson solution over a portion of the domain even at high Reynolds number, where agreement is not attained anywhere in the flow domain. This resemblance is apparent from the near zero angular velocities in the core for $r < 0.6$ as well as by the form of the radial velocity profiles over this same region.

3.4. *Comparison of numerical results with experiment*

Our intent, until now, has been to determine the validity of the similarity solution in describing flow between large but finite rotating disks. Our analysis of the flow is for arbitrarily large disks; thus, it is not assured that our results should describe the flow between finite disks of a given aspect ratio. We shall, in any event, compare our numerical results with experimental results reported in the literature. This comparison will be both quantitative, and when quantitative results are not available, qualitative.

We first make quantitative comparisons with some of the experimental data presented by Dijkstra & van Heijst (1983) for a closed-end system at an aspect ratio of 14. Figure 15 shows a comparison of experiment with our numerical results for azimuthal velocities, at two values of r, for $Re = 1000$, $s = 0$. The solid circles represent a summary of the experimental data, the curves are our numerical results. The experimental data were not taken at one specific value of r but rather over a

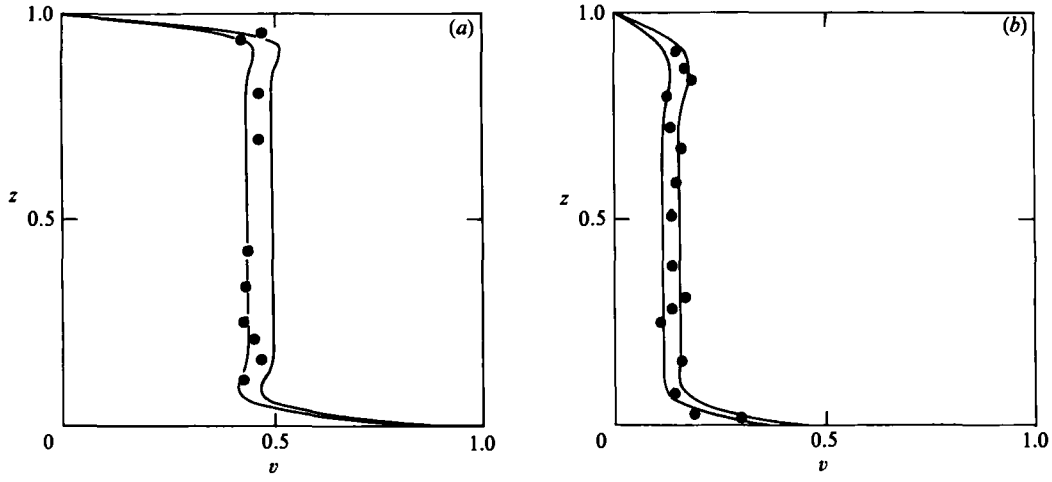

FIGURE 15. Comparison of numerical results (——) with the experimental results of Dijkstra & van Heijst (1983) (●) for azimuthal velocity at $Re = 1000$, $s = 0$, closed end: (*a*) $0.84 \leqslant r \leqslant 0.87$; (*b*) $0.36 \leqslant r \leqslant 0.45$. The experimental data were not taken at an exact value of r but over a small range.

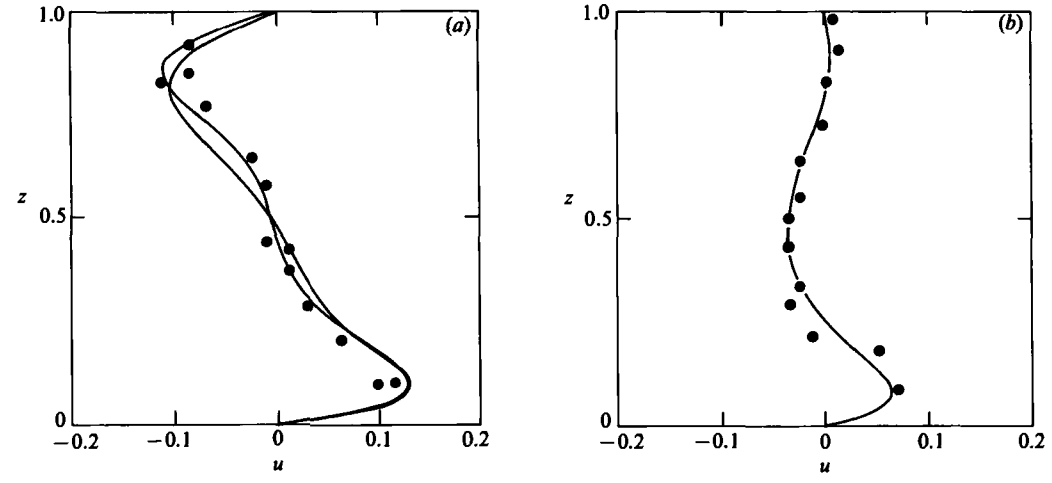

FIGURE 16. Comparison of numerical results (——) with the experimental results of Dijkstra & van Heijst (1983) (●) for radial velocity at $Re = 100$, $s = -0.3$, closed end: (*a*) $0.74 \leqslant r \leqslant 0.78$; (*b*) $r = 0.41$. The reversal of the direction of the radial velocity near the top disk is due to a stagnation point at $r = 0.70$.

small interval of r. The two curves are our numerical results at the interval boundaries; thus, the experimental data should fall between them. The agreement between experimentally measured azimuthal velocities and our numerical results is quite good, both at large ($0.84 \leqslant r \leqslant 0.87$) and at intermediate ($0.36 \leqslant r \leqslant 0.45$) radii. The agreement at large radius is a bit surprising because, for the experimental configuration used by Dijkstra & van Heijst, $H/L = 0.07$. Thus, even at a distance of only $2(H/L)$ away from the end, our asymptotic results agree with experiments performed at an aspect ratio of 14. In figure 16, a comparison of experimentally determined radial velocities with our numerical results is shown for $Re = 100$,

$s = -0.3$. Again the agreement is good. Note the change in sign of the radial velocity near the top disk between $r = 0.74$ and 0.41, indicating the existence of a stagnation point.

Dijkstra & van Heijst qualitatively observed Stewartson-type velocity profiles for strong counter-rotation at high Reynolds number ($Re \geqslant 500$). Specifically, they reported that for $s = -0.6$, $Re = 1000$ and $s = -4.5$, $Re = 500$ the angular velocity virtually vanished outside the disk boundary layers for $0 < r < 0.6$. Such behaviour was also noted for $s = -0.8$, $Re \geqslant 500$. However, at $s = -0.15$, $Re = 500$, Dijkstra & van Heijst observed a definite angular motion in the core fluid.

These observations are completely consistent with our numerical results. For strong counter-rotation at high Reynolds number, we find that the finite-disk closed-end flows resemble the Branch 4 similarity solution over a portion of the flow domain. Even in parameter ranges where the finite-disk flow is not described precisely by the similarity solution over any part of the flow domain (e.g. $s = -1$, $Re = 500$, closed end and $s = -0.8$, $Re > 120$, closed end), it tends to resemble the Stewartson-type (Branch 4) similarity solution over a portion of the domain. The structure of the similarity solution does not change over the region of s: $-1 < s < -\frac{1}{3}$. In this range of s, the solution, which extends from 0 to ∞ in Reynolds number, is the Branch 2 similarity solution, and Branches 3 and 4 appear at higher values of Re, as illustrated for $s = -0.8$ in figure 13. This explains the resemblance in behaviour observed by Dijkstra & van Heijst at high Reynolds number for $s = -0.8$, -0.6 and -0.45.

For $s = -0.15$, however, the structure of the similarity solution is quite different. Now, Branch 8 extends from $Re = 0$ to ∞ and other branches appear at higher Re. The structure of the similarity solution for $s = -0.15$ is analogous to that for $s = -0.25$, which is considered in detail in Durlofsky (1986). For these flows, the Branch 8 similarity solution is seen to be the similarity solution applicable to the flow between finite disks, and this solution does in fact display a bulk angular velocity, as observed by Dijkstra & van Heijst. Thus, the observations of Dijkstra & van Heijst are consistent with the finite-disk numerical results.

Picha & Eckert (1958) conducted experiments for both shrouded and unshrouded disk configurations. The largest aspect ratio they considered was nine, and the smallest Reynolds number considered, at this aspect ratio, was approximately 3200. Because our numerical results have not been extended beyond 1000, quantitative comparison is impossible. Qualitatively, Picha & Eckert observed zero core angular velocity for both shrouded and unshrouded disks when the disks were counter-rotated. This is consistent with our results, at least for $-1 \leqslant s < -0.25$. They also observed, for unshrouded disks, zero core angular velocity when one disk was rotated and the other was stationary, but a definite bulk angular velocity when the disks were enclosed. This too is in agreement with our findings.

Dijkstra & van Heijst also conducted some experiments to assess the effect of rotating versus not rotating the sidewall. Their results show that the rotation of the housing has virtually no effect on the location of the stagnation point and, for $0 \leqslant r \leqslant 0.7$, little effect on the angular velocity at $z = 0.5$ for $s = 0$. This is in agreement with our inviscid analysis of the end region.

4. Conclusions

The results of previous sections lead to many important conclusions concerning the flow between finite rotating disks. Of primary importance is the observation that the

end effect increased with increasing Reynolds number. The effect of the end was apparent as a deviation between the similarity solution and finite-disk flows. Because our analysis is valid for disks of arbitrarily large but finite radii, this result indicates that, regardless of the size of the disks, the effect of the end is not confined to a region near the end. Indeed, in most cases considered, for $Re \gtrsim 200$, quantitative agreement between the similarity solution and the finite-disk solution, if it existed at all, was over only a fraction of the flow domain, typically not beyond $r \approx 0.2$. In many cases, however, there was qualitative resemblance between the two over a larger region, perhaps up to $r \approx 0.6$. These results indicate that, for moderate- to high-Reynolds-number flows, the similarity solution may be useful as an approximation to the actual flow over the inner portion of the flow domain, say from $r = 0$ to 0.5, but not as a quantitative description of the flow except possibly in the immediate vicinity of the axis of rotation. At restricted values of axial position z, say within a boundary layer adjacent to a spinning disk, the similarity solution may give an accurate description of the flow, even though there is not agreement for all z.

Our results also show the importance of the type of end condition in determining the form of the flow throughout the domain between finite rotating disks. This was most apparent for the $s = 0$ flows where, at high Re ($Re \geqslant 250$), the end condition determined which similarity solution the flow resembled. The open-end flows, with incoming fluid of zero angular velocity and uniform radial velocity resembled the Stewartson solution, while the closed-end flows resembled the Batchelor solution. The importance of the angular velocity of the incoming fluid was also seen for $s = -1$ flows. When the angular velocity of the incoming fluid was set to correspond with the angular velocity of one of the asymmetric similarity solutions, the $s = -1$ finite-disk flow resembled the asymmetric similarity solution over a portion of the flow domain. As shown in Durlofsky (1986), the formation of a stagnation point in the $s = -0.25$ flows, as well as the structure of the flow throughout most of the domain, is also caused by the angular velocity of the returning fluid. Because of the relatively high-angular-velocity fluid in the vicinity of the slower moving top disk near the end $r = 1$, the closed-end flows formed stagnation points. The open-end flows, by contrast, did not because the incoming fluid near the top disk was of zero angular velocity.

In many of the finite-disk flows, collision regions formed at the axis of rotation. This occurred for $s = -1$ closed-end flows for $Re \geqslant 400$; for $s = -1$ flows with either end condition for $Re \geqslant 140$ after the introduction of an asymmetry; for $s = 0$ open-end flows for $Re \geqslant 250$; and for $s = -0.8$ closed-end flows for $Re \geqslant 200$. A collision region also formed for $s = -0.8$ open-end flows at high Re, but was attributed to our extrapolation procedure.

A collision region may form at the axis of rotation for one of two reasons. The flow may simply lack sufficient viscosity at high Re to damp the effect of the end. If the disturbance caused by the end does not decay as $r \to 0$, a collision region will form. This is the mechanism for collision-region formation for the $s = -1$ closed-end flows for $Re \geqslant 400$ and for the $s = -0.8$ closed-end flows for $Re \geqslant 200$. This effect was also observed by Brady (1984) and Brady & Acrivos (1982) in their studies of the flow in a channel or tube with either a uniformly porous surface or an accelerating surface. When a collision region forms by this mechanism, the finite-domain flow does not approach similarity form at intermediate values of r, though its velocity profiles may resemble qualitatively those of the similarity flow.

The other manner in which a collision region may form is more subtle. It occurs when the finite-disk solution approaches a temporally unstable similarity solution at

intermediate values of r. This may occur when the end condition resembles the temporally unstable similarity solution. Once the finite disk solution is 'sufficiently close' to the unstable similarity solution, which generally occurs for $0.2 \leqslant r \leqslant 0.4$, the instability manifests itself, giving rise to an abrupt deviation from similarity form and to the formation of a collision region. This will only occur, however, if the finite-disk flow possesses a component of the unstable mode. For the $s = 0$ open-end flows at $Re \geqslant 250$, the end condition apparently did excite the unstable mode. For the $s = -1$ flows, however, the end condition did not introduce any destabilizing disturbance. Upon directly applying a disturbance that was asymmetric about the midline, the unstable mode was excited and a collision region formed. The feature that distinguishes flows which form collision regions by this mechanism is their strong resemblance to the unstable similarity solution at intermediate values of r. Flows that form collision regions by the other mechanism never attain this degree of resemblance. In neither case, however, does the similarity solution provide a valid description of the flow anywhere in the domain between the finite rotating disks.

From the above discussion, it is apparent that temporally unstable similarity solutions are relevant to the description of the steady flow between finite rotating disks. This result in itself is significant because one probably would not expect correspondence between an unstable similarity solution and a steady finite-domain flow. Though they do not quantitatively describe finite-domain flows, unstable similarity flows represent, in some cases (e.g. $s = -1$ and -0.8, either end condition; $s = 0$, open end), the best similarity approximation to the flow over some region between finite rotating disks.

The $s = -0.8$ open-end finite-disk flows, for $Re \geqslant 200$, were seen to resemble two different similarity solutions over two different regions of the flow domain. At intermediate values of r, these flows resembled the unstable Branch 4 Stewartson solution, but nearer the axis of rotation they deviated from this form and resembled the Branch 2 similarity solution plus a small perturbation term associated with the Branch 2 solution. These flows were the only flows we found to exhibit such behaviour. We performed small perturbation analyses for the relevant similarity solutions at all values of s considered and attempted to resolve collision regions in terms of a similarity solution plus its small perturbation term. Only for the $s = -0.8$ open-end flow could we interpret the finite-disk collision region in this way. All other collision regions appear to vary more fundamentally from similarity form.

Though our intent in this study was to determine the validity of the von Kármán similarity solution in describing the flow between finite rotating disks, the procedure described in §2 may be relevant to many other problems. Our analysis of the end region could be generalized and applied to other large-aspect-ratio problems, eliminating the difficult numerical problem of resolving the details of the flow in a turning region. Within the context of rotating disk flows, several straightforward extensions of our work are feasible. Problems involving suction or injection at one or both disks or net throughflows could be handled with only minor changes to the formulation presented in §2. Also, using our calculated flow fields, the concentration and temperature fields in a fluid between rotating disks, which are of particular importance in many problems (e.g crystal growth), can be readily computed.

REFERENCES

ADAMS, M. L. & SZERI, A. Z. 1982 Incompressible flow between finite disks. *Trans. ASME* E: *J. Appl. Mech.* **49**, 1–9.

BATCHELOR, G. K. 1951 Note on a class of solutions of the Navier–Stokes equations representing steady rotationally-symmetric flow. *Q. J. Mech. Appl. Maths.* **4**, 29–41.

BATCHELOR, G. K. 1967 *An Introduction to Fluid Dynamics.* Cambridge University Press.

BIEN, F. & PENNER, S. S. 1970 Velocity profiles in steady and unsteady rotating flows for a finite cylindrical geometry. *Phys. Fluids* **13**, 1665–1671.

BÖDEWADT, U. T. 1940 Die drehstromung uber festem grunde. *Z. angew. Math. Mech.* **20**, 241–253.

BRADY, J. F. 1984 Flow development in a porous channel and tube. *Phys. Fluids* **27**, 1061–1067.

BRADY, J. F. & ACRIVOS, A. 1982 Closed-cavity laminar flows at moderate Reynolds number. *J. Fluid Mech.* **115**, 427–442.

CHEN, K. K. & LIBBY, P. A. 1968 Boundary layers with small departures from the Falkner–Skan profile. *J. Fluid Mech.* **33**, 273–282.

COCHRAN, W. G. 1934. The flow due to a rotating disk. *Proc. Camb. Phil. Soc.* **30**, 365–375.

DIJKSTRA, D. & HEIJST, G. J. F. VAN 1983 The flow between two finite rotating disks enclosed by a cylinder. *J. Fluid Mech.* **128**, 123–154.

DURLOFSKY, L. 1986 Topics in fluid mechanics: I. Flow between finite rotating disks II. Simulation of hydrodynamically interacting particles in Stokes flow. Ph.D. Thesis, Massachusetts Institute of Technology.

DURLOFSKY, L. & BRADY, J. F. 1984 The spatial stability of a class of similarity solutions. *Phys. Fluids* **27**, 1068–1076.

GREENSPAN, H. P. 1980 *The Theory of Rotating Fluids.* Cambridge University Press.

HARRIOTT, G. M. & BROWN, R. A. 1984 Flow in a differentially rotated cylindrical drop at moderate Reynolds number. *J. Fluid Mech.* **144**, 403–418.

HOLODNIOK, M., KUBICEK, M. AND HLAVACEK, V. 1977 Computation of the flow between rotating coaxial disks. *J. Fluid Mech.* **81**, 689–699.

HOLODNIOK, M., KUBICEK, M. & HLAVACEK, V. 1981 Computation of the flow between rotating coaxial disks: multiplicity of steady-state solutions. *J. Fluid Mech.* **108**, 227–240.

KÁRMÁN, T. VON 1921 Uber laminare und turbulente reibung. *Z. angew. Math. Mech.* **1**, 233–252.

LANCE, G. N. & ROGERS, M. H. 1962 The axially symmetric flow of viscous fluid between two infinite rotating disks. *Proc. R. Soc. Lond.* A**266**, 109–121.

LUGT, N. J. & HAUSSLING, H. J. 1973 Development of flow circulation in a rotating tank. *Acta Mech.* **18**, 255–272.

MELLOR, G. L., CHAPPLE, P. J. & STOKES, V. K. 1968 On the flow between a rotating and a stationary disk. *J. Fluid Mech.* **31**, 95–112.

NGUYEN, N. D., RIBAULT, J. P. & FLORENT, P. 1975 Multiple solutions for flow between coaxial disks. *J. Fluid Mech.* **68**, 369–388.

PAO, H. P. 1970 A numerical computation of a confined rotating flow. *Trans. ASME* E: *J. Appl. Mech.* **37**, 480–487.

PAO, H. P. 1972 Numerical solution of the Navier–Stokes equations for flows in the disk–cylinder system. *Phys. Fluids* **15**, 4–11.

PARTER, S. V. 1982 On the swirling flow between rotating coaxial disks: a survey. *MRC Technical Summary Rep. No.* 2332.

PEARSON, C. E. 1965 Numerical solutions for the time-dependent viscous flow between two rotating coaxial disks. *J. Fluid Mech.* **21**, 623–633.

PICHA, K. G. & ECKERT, E. R. G. 1958 Study of the air flow between coaxial disks rotating with arbitrary velocities in an open or enclosed space. In *Proc. 3rd US Natl. Cong. Appl. Mech.* pp. 791–798.

ROBERTS, S. M. & SHIPMAN, J. S. 1976 Computation of the flow between a rotating and a stationary disk. *J. Fluid Mech.* **73**, 53–63.

SCHULTZ-GRUNOW, F. 1935 Der reibungswiderstand rotierender scheiben in gehausen. *Z. angew. Math. Mech.* **14**, 191–204.

STEWARTSON, K. 1953 On the flow between two rotating coaxial disks. *Proc. Camb. Phil. Soc.* **49**, 333–341.

SZERI, A. Z., GIRON, A., SCHNEIDER, S. J. & KAUFMAN, H. N. 1983*a* Flow between rotating disks. Part 2. Stability. *J. Fluid Mech.* **134**, 133–154.

SZERI, A. Z., SCHNEIDER, S. J., LABBE, F. & KAUFMAN, H. N. 1983*b* Flow between rotating disks. Part 1. Basic flow. *J. Fluid Mech.* **134**, 103–131.

SZETO, R. K.-H. 1978 The flow between rotating coaxial disks. Ph.D. thesis, California Institute of Technology.

ZANDBERGEN, P. J. & DIJKSTRA, D. 1987 Von Kármán swirling flows. *Ann. Rev. Fluid Mech.* **19**, (to appear).